2. EXPLANATORY NOTES[1]

Shipboard Scientific Party[2]

INTRODUCTION

In this chapter, we have assembled information that will help the reader to understand the basis for our preliminary conclusions and also will help the interested investigator to select samples for further analysis. This information concerns only shipboard operations and analyses described in the site reports in the *Initial Reports* volume of the Leg 145 *Proceedings of the Ocean Drilling Program*. Methods used by various investigators for shore-based analyses of Leg 145 data will be detailed in the individual scientific contributions published in the *Scientific Results* volume.

Authorship of Site Chapters

The separate sections of the site chapters were written by the following shipboard scientists (authors are listed in alphabetical order, no seniority is implied):

Site Summary: Basov, Rea
Background and Scientific Objectives: Basov, Rea
Operations: Grout, Janecek
Lithostratigraphy: Arnold, Krissek, McKelvey, Owen, Snoeckx, Tiedemann
Petrology: Keller
Biostratigraphy: Barron, Beaufort, Gladenkov, Keigwin, Morley, Olafsson, Pak, Shilov
Paleomagnetism: Okada, Weeks
Sedimentation and Mass Accumulation Rates: Keigwin
Inorganic Geochemistry: Ingram, Pedersen
Organic Geochemistry: Stax
Physical Properties: Kotilainen, Roberts, Rutledge
Downhole Measurements: Bristow, DeMenocal, Dubuisson
Seismic-Lithologic Correlation: Hamilton, Rea
Summary and Conclusions: Basov, Rea

Following the text of all site chapters, summary core descriptions ("barrel sheets") and photographs of each core are presented in a section called "Cores."

Use of *Ma* vs. *m.y.*

1. *Ma* describes age and thus is equivalent to and replaces m.y.B.P. (million years Before Present); example, 35 to 40 Ma.

2. *m.y.* describes a duration and is used in sentences such as, "for five m.y. during the early Miocene."

Drilling Characteristics

Information concerning sedimentary stratification in uncored or unrecovered intervals may be inferred from seismic data and wireline-logging results and from an examination of the behavior of the drill string, as observed and recorded on the drilling platform. Typically, the harder a layer, the slower and more difficult it is to penetrate. A number of other factors may determine the rate of penetration, so it is not always possible to relate the drilling time directly to the hardness of the layers. Bit weight and revolutions per minute, recorded by the drilling recorder, also influence the penetration rate.

Drilling Deformation

When cores are split, many show signs of significant sediment disturbance, including the concave-downward appearance of originally horizontal bands, haphazard mixing of lumps of different lithologies (mainly at the tops of cores), and the near-fluid state of some sediments recovered from tens to hundreds of meters below the seafloor. Core deformation occurs during cutting, retrieval (with accompanying changes in pressure and temperature), and core handling on the deck of the ship.

SHIPBOARD SCIENTIFIC PROCEDURES

Numbering of Sites, Holes, Cores, and Samples

Ocean Drilling Program (ODP) drill sites are numbered consecutively and refer to one or more holes drilled while the ship was positioned over one acoustic beacon. Multiple holes may be drilled at a single site by pulling the drill pipe above the seafloor (out of the hole), moving the ship some distance from the previous hole, and then drilling another hole.

For all ODP drill sites, a letter suffix distinguishes each hole drilled at the same site. For example, the first hole drilled is assigned the site number modified by the suffix A, the second hole takes the site number and suffix B, and so forth. Note that this procedure differs slightly from that used by Deep Sea Drilling Project (DSDP) (Sites 1 through 624), but prevents ambiguity between site- and hole-number designations. It is important to distinguish among holes drilled at a site, because recovered sediments or rocks from different holes may not come from equivalent positions in the stratigraphic column.

The cored interval is measured in meters below seafloor (mbsf). The depth interval assigned to an individual core begins with the depth below the seafloor when the coring operation began and extends to the depth when the coring operation ended (see Fig. 1). For example, each coring interval is generally up to 9.5 m long, which is the length of a core barrel. Coring intervals may be shorter and may not necessarily be adjacent if separated by drilled intervals. In soft sediments, the drill string can be "washed ahead" with the core barrel in place, without recovering sediments. This is achieved by pumping water down the pipe at high pressure to wash the sediment out of the way of the bit and up the space between the drill pipe and the wall of the hole. If thin, hard, rock layers are present, then it is possible to get "spotty" sampling of these resistant layers within the washed interval and thus to have a cored interval greater than 9.5 m. When drilling hard rock, a center bit may replace the core barrel if it is thought necessary to drill without core recovery.

Cores taken from a hole are numbered serially from the top of the hole downward. Core numbers and their associated cored intervals in meters below seafloor usually are unique in a given hole; however, this may not be true if an interval must be cored twice because of

[1] Rea, D.K., Basov, I.A., Janecek, T.R., Palmer-Julson, A., et al., 1993. *Proc. ODP, Init. Repts.*, 145: College Station, TX (Ocean Drilling Program).

[2] Shipboard Scientific Party is as presented in list of participants preceding the contents.

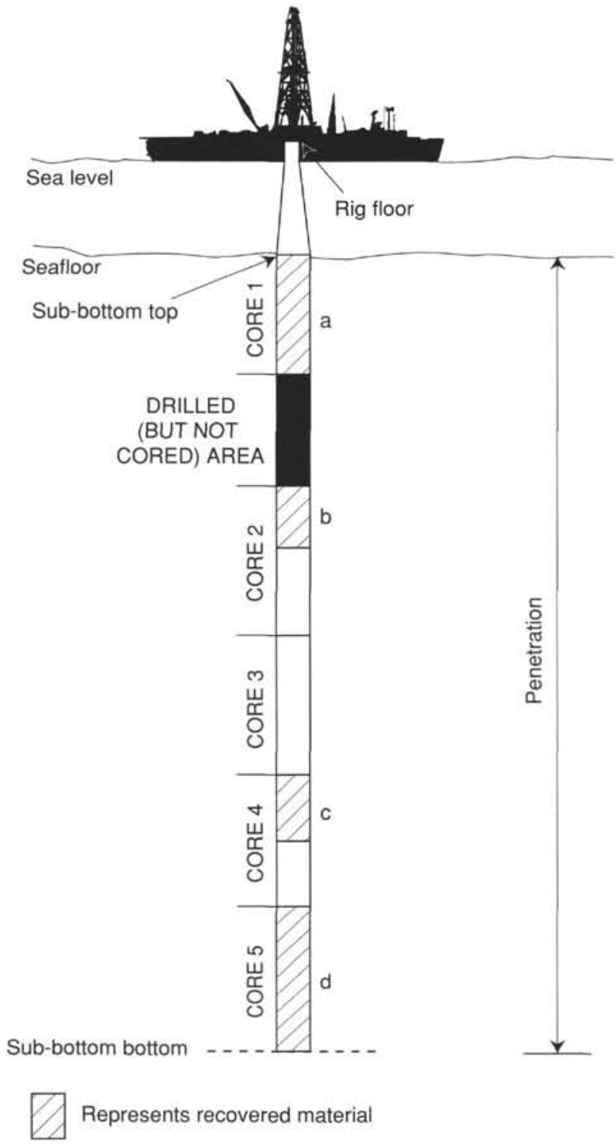

Represents recovered material

BOTTOM FELT: distance from rig floor to seafloor

TOTAL DEPTH: distance from rig floor to bottom of hole (sub-bottom bottom)

PENETRATION: distance from seafloor to bottom of hole (sub-bottom bottom)

NUMBER OF CORES: total of all cores recorded, including cores with no recovery

TOTAL LENGTH OF CORED SECTION: distance from sub-bottom top to sub-bottom bottom minus drilled (but not cored) areas in between

TOTAL CORE RECOVERED: total from adding a, b, c, and d in diagram

CORE RECOVERY (%): equals TOTAL CORE RECOVERED divided by TOTAL LENGTH OF CORED SECTION times 100

Figure 1. Coring and depth intervals.

caving of cuttings or other hole problems. Maximum complete recovery for a single core is 9.5 m of rock or sediment contained in a plastic liner (6.6-cm internal diameter) plus about 0.2 m (without a plastic liner) in the core catcher (Fig. 2). The core catcher is a device at the bottom of the core barrel that prevents the core from sliding out while the barrel is being retrieved from the hole. In certain situations (e.g., when coring gas-charged sediments, which expand while being brought on deck), recovery may exceed the 9.5-m maximum.

A recovered core is divided into 1.5-m sections that are numbered serially from the top (Fig. 2). When complete recovery is obtained, the sections are numbered from 1 through 7, with the last section possibly being shorter than 1.5 m (rarely, an unusually long core may require more than seven sections). When less than complete recovery is obtained, as many sections as needed to accommodate the length of the core will be recovered; for example, 4 m of core would be divided into two 1.5-m sections and a 1-m section. If cores are fragmented (recovery less than 100%), sections are numbered serially, and intervening sections are noted as void, whether shipboard scientists think that the fragments were originally contiguous or not. In rare cases, a section of less than 1.5 m may be cut to preserve features of interest (e.g., lithologic contacts).

By convention, material recovered from the core catcher is placed below the last section when the core is described and is labeled core catcher (CC); in sedimentary cores, this material is treated as a separate section. The core catcher is placed at the top of the cored interval in cases where material is recovered only in the core catcher. However, information supplied by the drillers or by other sources may allow for more precise interpretation about the correct position of core-catcher material within an incompletely recovered cored interval.

When the recovered core is shorter than the cored interval, the top of the core is equated with the top of the cored interval by convention to achieve consistency when handling analytical data derived from the cores. Samples removed from the cores are designated by distance measured in centimeters from the top of the section to the top and bottom of each sample removed from that section.

A complete identification number for a sample consists of the following information: leg, site, hole, core number, core type, section number, piece number (for hard rock), and interval in centimeters measured from the top of the section. For example, a sample identification of "145-881A-25X-1, 10–12 cm" would be interpreted as representing a sample removed from the interval between 10 and 12 cm below the top of Section 1, Core 25 (X designates that this core was taken during extended-core barrel drilling) of Hole 881A during Leg 145.

All ODP core and sample identifiers indicate core type. The following abbreviations are used:

R = rotary core barrel (RCB);
H = hydraulic piston core (HPC; also referred to as APC, or advanced hydraulic piston core);
P = pressure core barrel;
X = extended-core barrel (XCB);
B = drill-bit recovery;
C = center-bit recovery;
I = in-situ water sample;
S = sidewall sample;
W = wash-core recovery; and
M = miscellaneous material.

APC, XCB, RCB, and W cores were cut during Leg 145.

Core Handling

Sediments

As soon as a core was retrieved on deck, a sample was taken from the core catcher and given to the paleontological laboratory for an

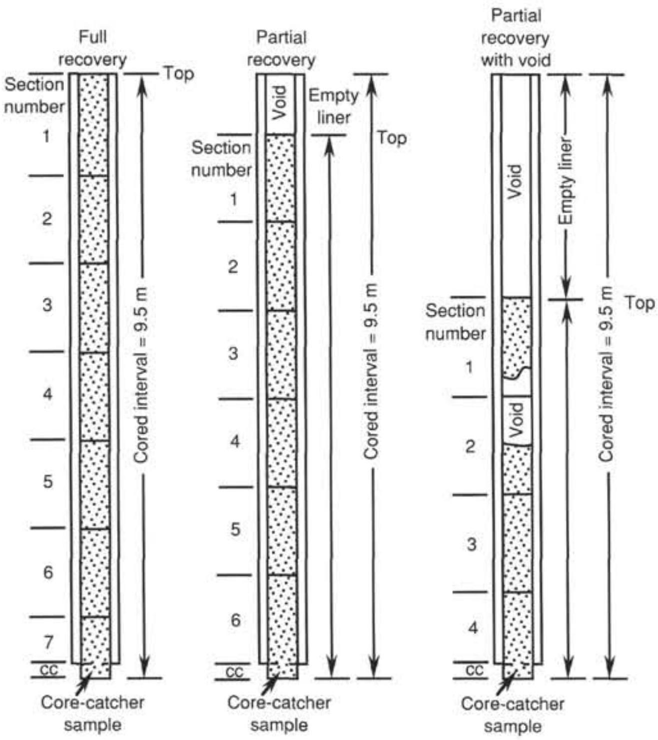

Figure 2. Examples of numbered core sections.

initial age assessment. Special care was taken when transferring the core from the drill floor to a long horizontal rack on a catwalk near the core laboratory so that the core did not bend or twist excessively. The core was capped immediately, and gas samples were taken by piercing the core liner and withdrawing gas into a vacuum tube. Voids within the core were sought as sites for gas sampling. Some of the gas samples were stored for shore-based study, but others were analyzed immediately as part of the shipboard safety and pollution-prevention program. Next, the core was marked into section lengths of 150 cm, each section was labeled, and the core was cut into sections. Interstitial-water (IW) and whole-round physical-properties (PP) samples were also taken at this time. In addition, on the catwalk some head-space gas samples were taken from the end of cut sections and sealed in glass vials for light hydrocarbon analysis. Afterward, each section was sealed at the top and bottom by gluing on color-coded plastic caps: blue to identify the top of a section and clear for the bottom. A yellow cap was placed on the section ends from which a whole-round sample was removed. The caps were usually attached to the liner by coating the end liner and the inside rim of the cap with acetone and then attaching the caps to the liners.

The cores then were carried into the laboratory, where the sections were labeled with an engraver to mark the complete designation of the section permanently. The length of the core in each section and the core-catcher sample were measured to the nearest centimeter; this information was logged into the shipboard CORELOG database program.

Whole-round sections from APC and XCB cores normally were run through the multisensor track (MST). The MST includes the gamma-ray attenuation porosity evaluator (GRAPE), the *P*-wave logger, and a volume magnetic susceptibility meter. After the core had equilibrated to room temperature (approximately 3 hr), thermal conductivities were measured in fairly soft sediments, and the cores were split.

Cores of soft material were split lengthwise into working and archive halves. The softer cores were split with a wire or saw, depending on the degree of induration. Harder cores were split with a band saw or diamond saw.

After splitting, working and archive halves of each section were designated. The archive halves of cores were first described visually. Smear slides were made from samples taken from the archive halves and were supplemented where necessary for hard rock descriptions by thin sections taken from the working halves. This analysis was followed by running the archive half of the core through the cryogenic magnetometer. Finally, the cores were photographed with both black-and-white and color film, a whole core at a time. Close-up photographs (black-and-white) were taken of particular features, as requested by individual scientists, for illustrations in the summary of each site. The archive halves of cores from the second complete hole at each site (generally the "B" hole) were first run through the cryogenic magnetometer to provide scientists sampling physical properties guidance when choosing sample intervals. The archive halves then were described visually and, finally, photographed.

The working half of each core was first measured for sonic velocity and vane shear strength. (During coring at the second complete hole at each site, these measurements were not performed until after the preliminary paleomagnetic data were available to avoid sampling in intervals of paleomagnetic interest.) After physical-properties sampling, the working half was sampled for reconnaissance-level and low-resolution shipboard and shore-based laboratory studies.

Each sample extracted was logged into the sampling database program by the location and the name of the investigator receiving the sample. Records of all of the samples removed are kept by the curator at ODP headquarters. The extracted samples were sealed in plastic vials or bags and labeled. Samples were routinely taken for shipboard physical-property analyses. Subsequently, these samples were used for calcium carbonate (coulometric) and organic carbon (CNS elemental) analyses; these data are reported in the site chapters.

Both halves of each core were placed into labeled plastic tubes, which then were sealed and transferred to cold-storage space aboard the drilling vessel. At the end of the leg, the cores were transferred from the ship in refrigerated air-freight containers to cold storage at the Gulf Coast Repository of the Ocean Drilling Program, Texas A&M University, College Station, Texas.

VISUAL CORE DESCRIPTIONS

Sediment "Barrel Sheets"

The visual core description forms (Fig. 3), or "barrel sheets," summarize the data obtained during shipboard analysis of each sediment core. The following discussion explains the ODP conventions used for compiling each part of the visual core description forms and the exceptions to these procedures adopted by the Leg 145 shipboard scientific party.

Shipboard sedimentologists were responsible for visual core logging, smear slide analyses, and thin section descriptions of sedimentary and volcaniclastic material. Mineral composition data, determined by X-ray diffraction (XRD), were used in some cases to augment the visual core descriptions. Data for biostratigraphy (age), geochemistry ($CaCO_3$, C_{org}, X-ray fluorescence [XRF]), paleomagnetism, and physical properties (wet-bulk density and porosity) were integrated with the sedimentological information.

In addition to the sedimentological information in the barrel sheets, plots of the gamma-ray attenuation porosity evaluator (GRAPE) and magnetic susceptibility data are displayed next to the traditional barrel sheet information (Fig. 3). The GRAPE and magnetic susceptibility data were available before the core was described, and sediments corresponding to specific features on these records were occasionally examined to determine their origin.

Core Designation

Cores were designated using leg, site, hole, core number, and core type, as discussed in a preceding section (see "Numbering of Sites, Holes, Cores, and Samples" section, this chapter). The cored interval

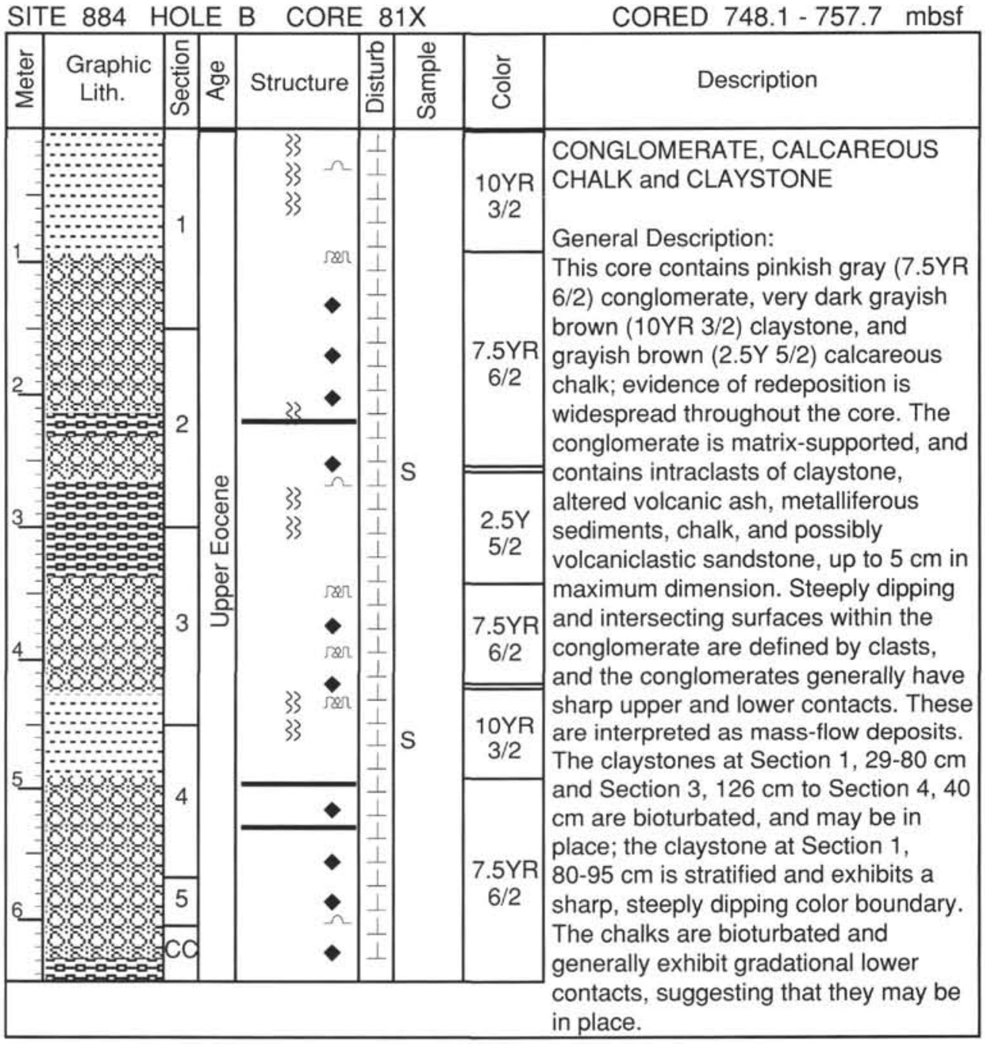

Figure 3. Example of core description form ("barrel sheet") used for describing sediments and sedimentary rocks.

has been specified in terms of meters below sea level (mbsl) and meters below seafloor (mbsf). On the basis of drill-pipe measurements (dpm), reported by the SEDCO coring technician and the ODP operations superintendent, depths have been corrected for the height of the rig-floor dual-elevator stool above sea level to give true water depth and correct depth below sea level.

Chronostratigraphy

The chronostratigraphic unit, as recognized on the basis of paleontological results, is shown in the "Age" column. Detailed information about biostratigraphic zonations is presented in the "Biostratigraphy" section in each site report.

"Graphic Lithology" Column

The lithology of the material recovered is represented in the core description forms by up to three symbols in the column titled "Graphic Lithology." The symbols used to represent each lithologic component are shown in Figure 4. Where an interval of sediment or sedimentary rock was a homogeneous mixture, the constituent categories have been separated by a solid vertical line, with each category represented by its own symbol. Constituents accounting for <25% of the sediment in a given lithology have not been shown in the "Graphic Lithology" column, but have been listed in the "Lithologic Description" column of the barrel sheet. In an interval comprising two or more sediment lithologies that have different compositions, such as in thin-bedded and highly variegated sediments, the average relative abundances of the lithologic constituents have been represented graphically by dashed lines that vertically divide the interval into appropriate fractions, as described above. The "Graphic Lithology" column shows only the composition of layers or intervals that exceed 20 cm in thickness.

Sedimentary Structures

In sediment cores, natural structures and structures created by the coring process can be difficult to distinguish. Natural structures observed have been indicated in the "Structure" column of the visual core description form. This column has been divided into three vertical areas for symbols (Fig. 5). The symbols on the left side of the "Structure" column indicate the location and relative thickness of ash layers in the sediment. The intensity of bioturbation is shown in the central portion of the "Structure" column of the barrel sheet in the conventional manner (slight, moderate, heavy). The symbols on the right side of the "Structure" column indicate the location of individual bedding features and any other sedimentary features, (such as nodules, zeolite crystals, ash layers, and shell fragments). The symbols used to describe each of these primary and secondary biogenic and physical sedimentary structures are shown in Figure 6.

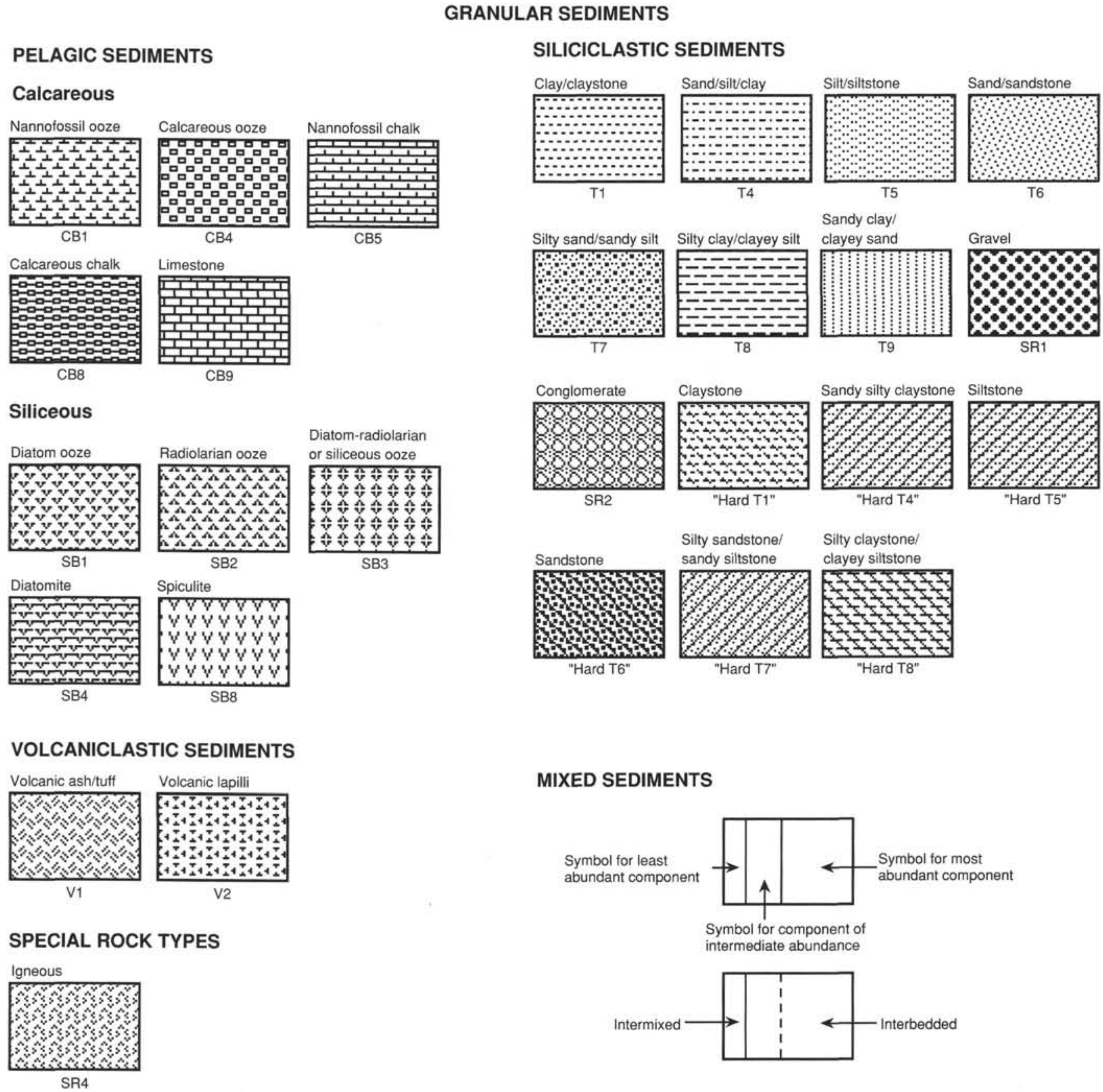

Figure 4. Sediment lithology/lithologic component symbols used in the "Graphic Lithology" column on the core description form shown in Figure 3.

Sedimentary Disturbance

Sediment disturbance resulting from the coring process is illustrated in the "Disturbance" column on the core description form (using symbols in Fig. 7). Blank regions indicate absence of drilling disturbance. The degree of drilling disturbance is described for soft and firm sediments, using the following categories:

1. Slightly deformed: bedding contacts are slightly bent;
2. Moderately deformed: bedding contacts have undergone extreme bowing;
3. Highly deformed: bedding is completely disturbed, sometimes showing symmetrical diapirlike or flow structures; and
4. Soupy: intervals are water-saturated and have lost all aspects of original bedding.

The degree of fracturing in indurated sediments and igneous rocks is described using the following categories:

1. Slightly fractured: core pieces are in place and contain little drilling slurry or breccia;
2. Moderately fragmented: core pieces are in place or partly displaced, but original orientation is preserved or recognizable (drilling slurry may surround fragments);
3. Highly fragmented: pieces are from the interval cored and probably in correct stratigraphic sequence (although they may not

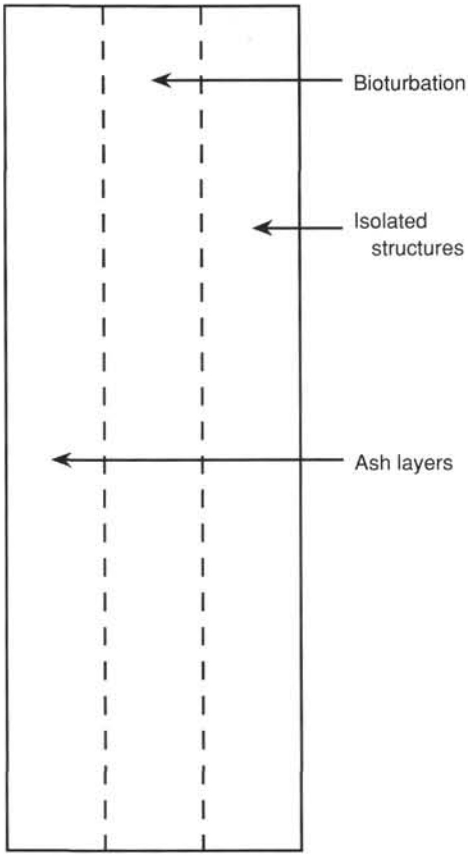

Figure 5. Layout of "Structures" column on the core description form shown in Figure 3.

represent the entire section), but original orientation has been completely lost; and

4. Drilling breccia: core pieces have lost their original orientation and stratigraphic position and may be mixed with drilling slurry.

Induration

The criteria used to determine the induration of pelagic sediments found during Leg 145 are subjective and provide three classes for pelagic oozes:

1. Soft: sediments that have little strength and are readily deformed under the finger or broad blade of the spatula are termed oozes or clay;
2. Firm: partly lithified pelagic sediments, such as oozes or clays, are readily deformed under the fingernail or the edge of a spatula blade; and
3. Hard: nonfriable, cemented rocks.

The suffix "-stone" is added to the name of cemented rocks (e.g., limestone, claystone). Hard siliceous sedimentary rocks are called chert or porcellanite.

Color

The hue and chroma attributes of color were determined using a Minolta CM-2002 color scanner as soon as possible after the cores were split, because redox-associated color changes may occur when deep-sea sediments are exposed to the atmosphere. Core color, in standard Munsell notation, is given in the "Color" column on the core description form.

Samples

The position of samples taken from each core for shipboard analysis is indicated in the "Samples" column on the core-description form (Fig. 3). The symbol "S" indicates the location of smear-slide samples; the symbol "T" indicates the location of thin-section samples; and the symbol "M" indicates the location of paleontology samples. The notations "I" and "P" designate the locations of samples for whole-round interstitial water geochemistry and physical properties analysis, respectively. The symbol "D" indicates the location of samples taken for XRD analysis.

Smear Slide Summary

A figure summarizing data from smear slides appears in each site chapter, and a table summarizing data from smear slides and thin sections appears at the end of each site chapter. This table includes information about the sample location; whether the sample represents a dominant ("D") or a minor ("M") lithology in the core; and the estimated percentages of sand, silt, and clay, together with all identified components. Note that smear slide analyses tend to underestimate the abundance of foraminifers and volcaniclastic-detrital material because these larger grains are difficult to incorporate into the smear.

Lithologic Description—Text

The lithologic description that appears on each core description form (barrel sheet) consists of three parts: (1) a heading that lists all the major sediment lithologies (see "Sedimentology" section, this chapter) observed in the core; (2) a heading for minor lithologies, and (3) a more detailed description of these sediments, including the locations of significant features in the core.

SEDIMENTOLOGY

Classification of Sediments and Sedimentary Rocks

During Leg 145, a modified version of the sediment classification scheme of the Ocean Drilling Program (Shipboard Scientific Party, 1990; Mazzullo et al., 1987) was used for granular sediment types (Fig. 8). Variations in the relative proportions of pelagic, siliciclastic, and pyroclastic grain types define four major classes of granular sediments: pelagic, siliciclastic, pyroclastic, and mixed (Fig. 8). The neritic class of sediments is not considered further here because a neritic component (e.g., bioclasts and shallow-water benthic foraminifers) was not recovered during Leg 145. Pelagic grains are the skeletal remains of open-marine siliceous and calcareous microfauna and microflora (e.g., radiolarians, diatoms, planktonic foraminifers, nannofossils) and associated organisms. Siliciclastic grains are mineral and rock fragments derived from igneous (plutonic and volcanic), sedimentary, and metamorphic rocks. Volcaniclastic grains include those of pyroclastic (direct products of magma degassing) and epiclastic (detritus derived from erosion of volcanic rocks) origins.

A granular sediment is classified by designating a principal name and major and minor modifiers. The principal name of a granular sediment defines its granular-sediment class; the major and minor modifiers describe the texture, composition, and fabric (Fig. 8).

Principal Names

For siliciclastic sediments, the principal name describes the texture and is assigned according to the following guidelines:

1. The Udden-Wentworth grain-size scale (Wentworth, 1922; Fig. 9) defines grain-size ranges and names of the textural groups (gravel, sand, silt and clay) and subgroups (fine sand, coarse silt, etc.) that are used as the principal names of siliciclastic sediments.

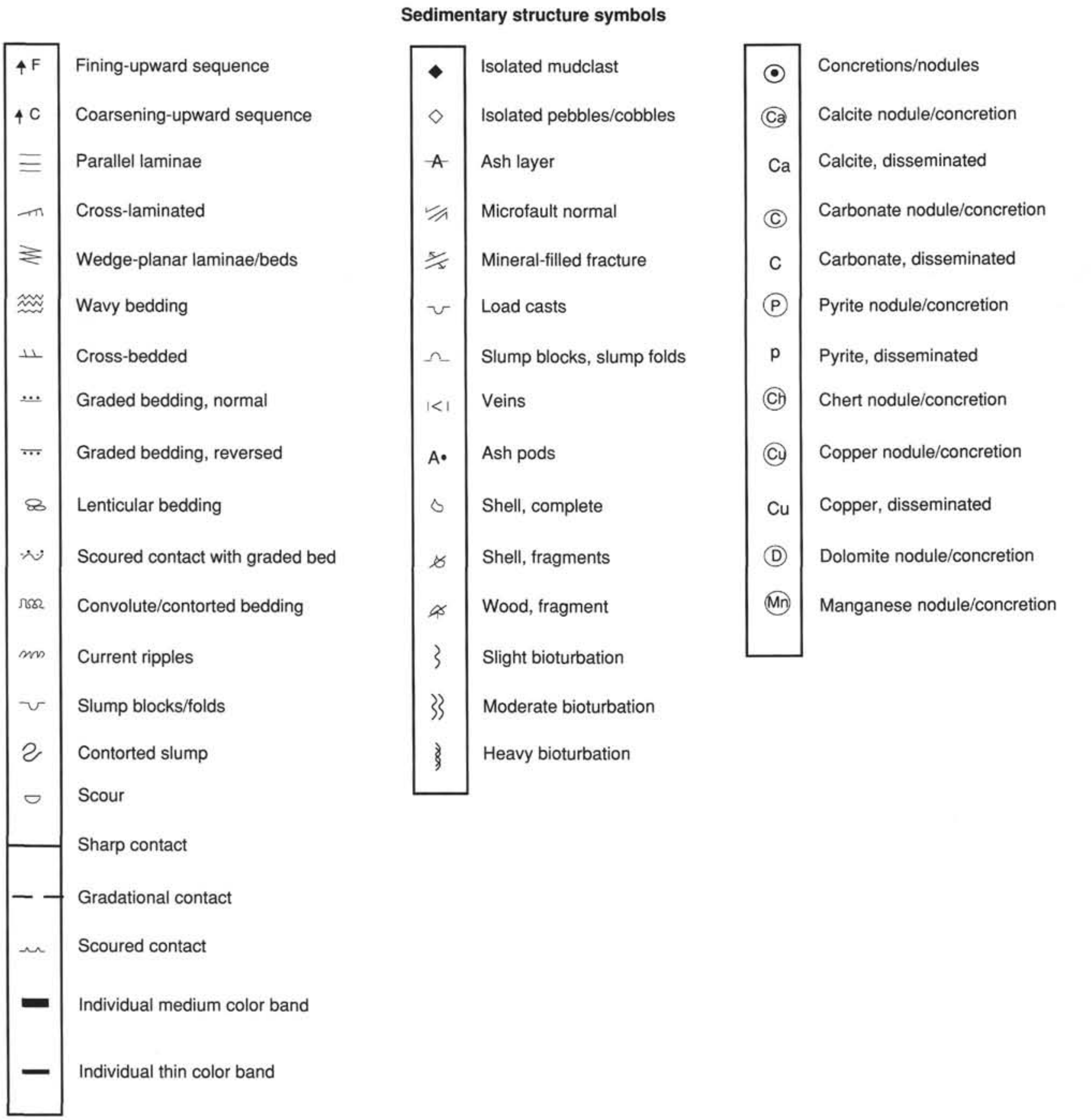

Figure 6. Sedimentary structure symbols used in the "Structures" column on the core description form shown in Figure 3.

2. Principal names are listed in order of increasing abundance when two or more textural groups or subgroups are present in a siliciclastic sediment (Shepard, 1954; Fig. 10). For simplicity, we have grouped intermediate mixtures of the three textural end members (sand, silt, and clay), into four categories (i.e., sandy clay/clayey sand, silty clay/clayey silt, silty sand/sandy silt, sandy silty clay).

3. The suffix "-stone" is affixed to the principal names sand, silt, and clay when the sediment is lithified. Conglomerate and breccia are used as principal names of lithified gravels having well-rounded and angular clasts, respectively.

Volcaniclastic sediments are subdivided into two groups, pyroclastic and epiclastic, with the principal name in each group describing texture. The names and ranges of three textural groups for pyroclastic sediments/rocks (Fisher and Schmincke, 1984) are as follows:

1. Volcanic breccia: pyroclasts >64 mm in diameter;
2. Volcanic lapilli: pyroclasts between 2 and 64 mm in diameter; when lithified, use the name lapillistone; and
3. Volcanic ash: pyroclasts <2 mm in diameter; when lithified, use the name tuff. For Leg 145, this group was subdivided into two classes by grain size: coarse ash/tuff, having grains between 1/16 and 2 mm in size, and fine ash/tuff, having grains <1/16 mm in size.

Epiclastic sediments, like siliciclastic sediments, have been classified based on grain texture, according to the Udden-Wentworth grain-

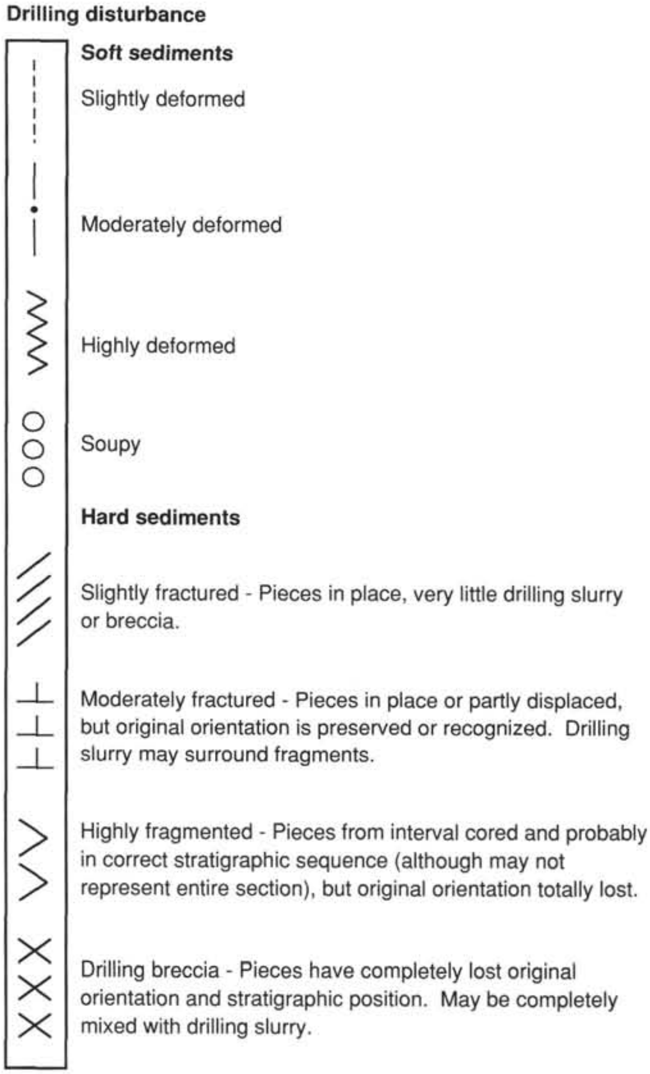

Figure 7. Drilling disturbance symbols used in the "Disturbance" column on the core description form shown in Figure 3.

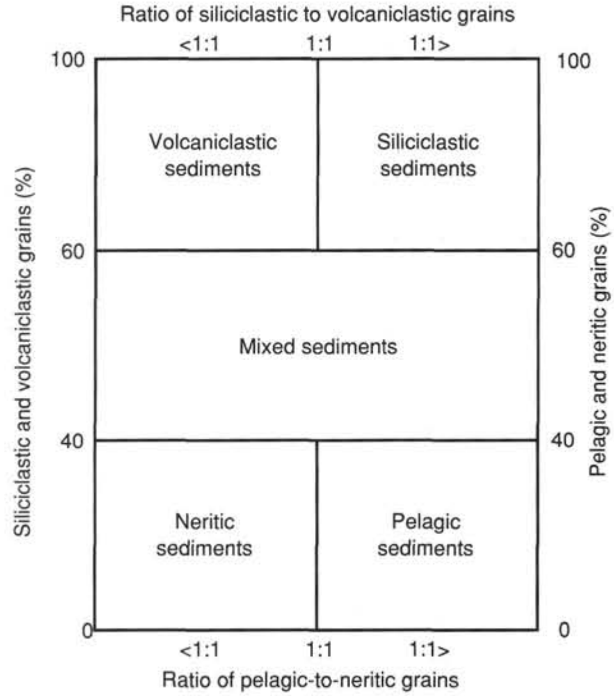

Figure 8. Diagram showing classes of granular sediment (modified from Mazzullo et al., 1987).

size scale. The textural principal name is preceded by the modifier "volcaniclastic" (e.g., volcaniclastic conglomerate, volcaniclastic sand). Other rules apply (as listed above) for siliciclastic sediments. Compositional modifiers have been added to the name as necessary (e.g., felsic, mafic, basaltic, etc.).

For pelagic sediment, the principal name describes the composition and degree of consolidation using the following terms:

1. Ooze: unlithified calcareous and/or siliceous pelagic sediments;
2. Chalk: partially lithified pelagic sediment, predominantly composed of calcareous pelagic grains;
3. Limestone: lithified pelagic sediment, predominantly composed of calcareous pelagic grains;
4. Radiolarite, diatomite, and spiculite: partially lithified pelagic sediment, predominantly composed of siliceous radiolarians, diatoms, and sponge spicules, respectively; and
5. Chert: lithified pelagic sediment, predominantly composed of recrystallized siliceous pelagic grains.

Major and Minor Modifiers

The principal name of a granular-sediment class is preceded by major modifiers and followed by minor modifiers (preceded by "with") that describe the lithology of the granular sediment in greater detail. Major and minor modifiers are used most commonly to describe composition and textures of grain types present in major (>25%) and minor (10%–25%) proportions and to describe grain fabric (e.g., matrix-supported).

Composition of pelagic grains can be described with the major and minor modifiers diatom(-aceous), radiolarian, spicule(-ar), siliceous, nannofossil, foraminifer(-al), and calcareous. The terms siliceous and calcareous are used generally to describe sediments composed of siliceous or calcareous pelagic grains of mixed origins. Sediment fabric can be described by the major modifiers, grain-supported or matrix-supported. In general, fabric descriptors are applied only to gravels, conglomerates, and breccias.

The degree of consolidation is described using the following major modifiers: "unlithified" designates soft sediment that is readily deformable under the pressure of a finger, "partially lithified" designates firm sediment that is incompletely lithified, and "lithified" designates hard, cemented sediment that must be cut with a saw.

Grain shapes are described by the major modifiers rounded, subrounded, subangular, and angular. Sediment color is determined relative to the Munsell Chart, a standard color-comparator, and can be employed as a major modifier.

Mixed sediments are described using major and minor modifiers that indicate composition and texture.

X-ray Diffraction Methods

Selected samples were analyzed on board the ship using X-ray diffraction techniques. Bulk samples were freeze-dried, ground by hand in a mortar and pestle, and mounted as back-loaded pressed powders in standard sample holders. X-ray diffraction patterns of these specimens were produced using the shipboard Philips AD 3420 X-ray diffractometer (CuK alpha emission). Peaks were visually inspected and matched to standard reference peaks for various minerals (quartz, 4.24Å and 3.34Å; feldspar, 4.04Å and 3.18Å; calcite, 3.03Å; smectite/chlorite, 14Å; illite, 10Å; chlorite, 7Å; etc.). The relative abundance of each mineral was estimated semiquantitatively

Millimeters		μm	Phi (Ø)	Wentworth size class	
			-20		
	4096		-12	Boulder (-8 to -12 Ø)	
	1024		-10		
	256		-8		
	64		-6	Cobble (-6 to -8 Ø)	
	16		-4	Pebble (-2 to -6 Ø)	
	4		-2		Gravel
	3.36		-1.75		
	2.83		-1.50	Granule	
	2.38		-1.25		
	2.00		-1.00		
	1.68		-0.75		
	1.41		-0.50	Very coarse sand	
	1.19		-0.25		
	1.00		0.00		
	0.84		0.25		
	0.71		0.50	Coarse sand	
	0.59		0.75		
1/2	0.50	500	1.00		
	0.42	420	1.25		
	0.35	350	1.50	Medium sand	Sand
	0.30	300	1.75		
1/4	0.25	250	2.00		
	0.210	210	2.25		
	0.177	177	2.50	Fine sand	
	0.149	149	2.75		
1/8	0.125	125	3.00		
	0.105	105	3.25		
	0.088	88	3.50	Very fine sand	
	0.074	74	3.75		
1/16	0.0625	63	4.00		
	0.0530	53	4.25		
	0.0440	44	4.50	Coarse silt	
	0.0370	37	4.75		
1/32	0.0310	31	5	Medium silt	
1/64	0.0156	15.6	6	Fine silt	
1/128	0.0078	7.8	7	Very fine silt	
1/256	0.0039	3.9	8		Mud
	0.0020	2.0	9		
	0.00098	0.98	10		
	0.00049	0.49	11	Clay	
	0.00024	0.24	12		
	0.00012	0.12	13		
	0.00006	0.06	14		

Figure 9. Udden-Wentworth grain-size scale for siliciclastic sediments (Wentworth, 1922).

using the maximum intensity measured for the corresponding peak; relative abundance ratios were estimated semiquantitatively by calculating the intensity ratios of the corresponding peaks. The abundance of amorphous and/or poorly crystalline silica, present either as biogenic opal or as volcanic ash, was estimated by using the difference in diffractogram background intensities at approximately 7Å and 3.34Å. The siliceous component represented by that shift in background intensity was identified by smear-slide analysis of the bulk sediment.

X-ray Fluorescence Methods

The trace-element compositions of selected sediment samples were analyzed on board the ship during Leg 145 using X-ray fluorescence (XRF) techniques. Because the sediments analyzed were relatively unlithified, sample preparation for trace-element analysis was as follows: samples were freeze-dried, briefly crushed in tungsten-carbide grinding vessels (duration less than 30 s), and formed into pellets in a SPEX press with a 31-mm steel pellet die, using polymer as a binder. The shipboard XRF system, its operating conditions, and the elements analyzed are discussed further in the "Igneous Petrology" section (this chapter).

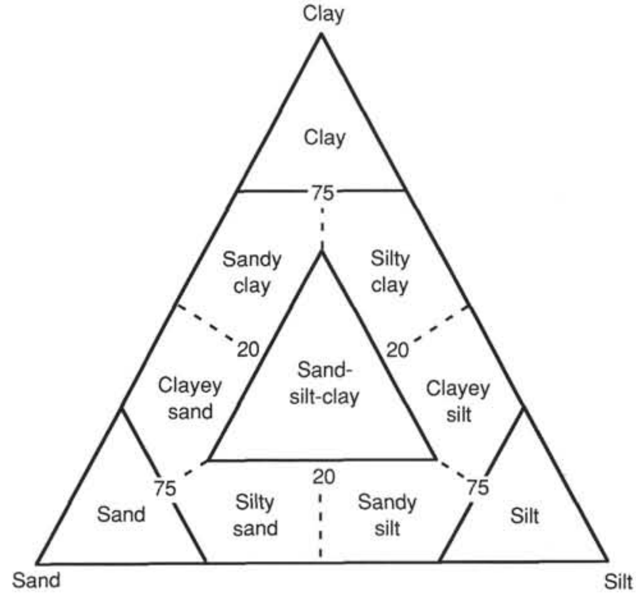

Figure 10. Ternary diagram showing principal names for siliciclastic sediments (modified from Shepard, 1954).

IGNEOUS PETROLOGY

Core Curation and Shipboard Sampling

Each igneous rock core was divided into 1.5-m sections. Each section was numbered, and each piece of rock in a section was numbered sequentially beginning with the number 1 at the top of each section. Pieces that could be fitted together were assigned the same number, followed by a consecutive letter (e.g., 1A, 1B, 1C, etc.). Plastic spacers were placed between pieces having different numbers, but not between pieces having the same number and different letters. The presence of a spacer represents an unknown, and possibly substantial, interval of no recovery. Any piece that was longer than the diameter of the core liner (i.e., the piece could not have rotated about a horizontal axis in the liner) was marked with a red wax cross on its base. Each piece was then split into archive and working halves using a rock saw with a diamond blade. Whenever possible, the cut was positioned so that each half contained representative samples of important features and structures. Core descriptions, photographs, and nondestructive measurements of magnetic susceptibility and thermal conductivity were performed using the archive halves. Samples for shipboard analyses (physical properties, magnetics, X-ray diffraction [XRD], X-ray fluorescence [XRF], and thin-section studies) and shore-based analyses were taken from the working half of the core.

Visual Core Descriptions

Basement hard rock cores were described on visual core description (VCD) forms specific to igneous and metamorphic rocks (see "barrel sheets" in the "Core" section, this volume). The VCD form for fine and medium-grained igneous rocks required the following information:

1. The leg, site, hole, core number and type, and section number;
2. A graphical representation of the core, including rock piece numbers and positions of shipboard samples;

3. Positions of lithologic unit boundaries, based on criteria such as the occurrence of glassy or quenched margins, marked trends of grain-size variation, and changes in petrographic type and phenocryst assemblages. If the contact was recovered, its location was recorded by core, section, position (cm), piece number, and unit number. When the contact was not recovered but a change of lithology was observed, the contact was placed at the base of the lowest piece in the lithologic unit.

The left column of the VCD is a graphical representation of the archive half. A horizontal line across the entire width of this column denotes a plastic spacer glued inside the liner. The number of each piece is also indicated. Oriented pieces are indicated by an upward-pointing arrow to the right of the piece. Shipboard samples are indicated in the "Shipboard Studies" column, using the following notation:

XRD = X-ray diffraction analysis,
XRF = X-ray fluorescence analysis,
PMAG = Magnetic measurements,
TS = Thin-section, and
PP = Physical properties measurement.

Core descriptions followed a checklist of macroscopic features to ensure consistent and complete descriptions. For each lithologic unit defined, the following checklist was used:

1. UNIT number (consecutive downhole), including piece numbers of top and bottom pieces in unit.
2. ROCK NAME (to be filled in later).
3. CONTACT TYPE: intrusive, chilled, discordant, depositional, etc. Note the dip of the contact.
4. PHENOCRYSTS: determine if homogeneous or heterogeneous through unit. List the following for each phenocryst phase: abundance (%), average size (in mm), shape (anhedral, subhedral, euhedral), degree of alteration (%), type of secondary phases, any other comments;

Now fill in ROCK NAME Item 2, above as follows:

5. GROUNDMASS TEXTURE: glassy, microcrystalline, fine-grained (<1.0 mm), medium-grained (1.0–5.0 mm). Note any relative grain-size changes within unit from piece to piece.
6. COLOR (dry).
7. VESICLES: size, shape, percentage, distribution and nature of any infillings.
8. STRUCTURE: massive, pillowed, thin or sheet-like, brecciated.
9. ALTERATION: type, form, distribution and degree, from fresh (<2% alteration present) to slightly altered (2%–10%), moderately altered (10%–40%), highly altered (40%–80%), very highly altered (80%–95%), and completely altered (95%–100%).
10. VEINS/FRACTURES: type, width, orientation, and nature of infillings.

Igneous rocks were named mainly on the basis of mineralogy and texture. Basalts (fine-grained) and dolerites (medium-grained) were termed aphyric if they contain <1% phenocrysts. If porphyritic, the rock may be sparsely phyric (phenocryst content of 1%–2%), moderately phyric (2%–10%), or highly phyric (>10%). Estimates of phenocryst proportions were based on those visible with a 10x hand lens. Basalts were further classified by phenocryst type: a moderately plagioclase-olivine phyric basalt contains 2%–10% total phenocrysts, most of which are plagioclase with lesser amounts of olivine.

Finally, any other comments may be added, including continuity of the unit within the core and inter-relationships among units. When the VCD form was complete, the information was put into the VAX computer database HARVI. Each record was checked by the database program for consistency and converted into a format that could be directly pasted onto the final VCD record for subsequent curatorial handling.

Thin-section Descriptions

Petrographic descriptions, including estimates of the various mineral phases (both primary and secondary), were made on the igneous thin-section description forms, and were put into the VAX computer database HRTHIN. Identifications of secondary phases, such as clays, zeolites, and infillings, were usually augmented by XRD (Brindley and Brown, 1980).

X-ray Diffraction Analysis

A Philips ADP 3720 X-ray diffractometer was used for the XRD analysis of unknown, generally secondary, mineral phases. Instrument conditions were as follows: CuK-alpha radiation with Ni filter, 40 kV, 35 mA, goniometer scan from 2° to 70° (2θ), with a 0.01° 2θ step size, and 0.5 s count time per step.

Samples were prepared by grinding in an agate mortar and pestle and mounted in aluminum sample holders. Glycolated samples (using ethylene glycol solution) were used to identify specific clay minerals.

X-ray Fluorescence Analysis

Samples that appeared to be representative of individual lithologic units or appeared to be of unusual composition were selected for geochemical analysis using X-ray fluorescence (XRF). The shipboard XRF system is a fully automated, wavelength-dispersive, ARL 8420 spectrometer using a 3-kW rhodium X-ray tube as the excitation source. A list of analyzed elements and operating conditions is given in Table 1. Rough seas and technical problems limited the use of the XRF to trace-element analyses only, and to basement samples only from Sites 883 and 884.

XRF samples were removed from the working half of the core using a diamond-bladed rock saw. Saw marks on the samples were removed by grinding on a wet resin-bonded diamond grinding disk. Each sample was then ultrasonically washed in methanol for 10 min, followed by three ultrasonic washings of 10 min each in deionized distilled water, and finally dried at 110°C for 2 hr. Large pieces were reduced to a <1 cm diameter by crushing between two plastic plates in a hydraulic press. The pieces then were powdered for 2 min or less in a Spex shatterbox having tungsten-carbide grinding vessels.

Trace elements were determined on pressed-powder pellets made by mixing approximately 8 cm^3 of rock powder with 30 drops of Chemplex Liquid Binder. This mixture was then pressed into an aluminum cap using seven tons of pressure. A minimum of 5 g of sample ensured that the pellet was "infinitely thick" for rhodium K-series radiation. Concentrations of trace elements were computed from measured X-ray intensities using a calibration curve derived from the measurement of well-analyzed reference rocks (BHVO-1, G-2, AGV-1, JGB-1, JP-1, Br, and DRN), and an off-line calculation program based on routines from Bougault et al. (1977) and written by T.L. Grove and M. Loubet. Background was determined either on blanks or derived by regression analysis from the calibration curves. Instrument drift was compensated for by including an internal standard in every run and by normalizing to its accepted value, and using that correction factor on unknowns in that same run. The results of repeated analyses of standard DRN during Leg 145 are given in Table 2.

Loss-on-ignition values were determined by drying the sample powders at 110°C for 8 hr and then weighing them before and after ignition at 1000°C.

BIOSTRATIGRAPHY

Time Scale/Chronological Framework

Because Leg 145 used Cande and Kent's (1992) geomagnetic polarity time scale, ages for biostratigraphic datums that had been calibrated to the Berggren, Kent, and Flynn (1985) and Berggren, Kent, and Van Couvering (1985) time scales had to be converted. This

Table 1. Leg 145 XRF analytical conditions.

Element	Line	Crystal	Detector	Collimator	Peak angle (deg)	Background offset (deg)	Total count time Peak	Total count time Background
Rh	K-C	LiF(200)	Scint	Fine	18.60	0	60	0
Nb	Kα	LiF(200)	Scint	Fine	21.39	±0.35	200	200
Zr	Kα	LiF(200)	Scint	Fine	22.54	±0.35	100	100
Y	Kα	LiF(200)	Scint	Fine	23.79	±0.40	100	100
Sr	Kα	LiF(200)	Scint	Fine	25.14	±0.41	100	100
Rb	Kα	LiF(200)	Scint	Fine	26.61	±0.60	100	100
Zn	Kα	LiF(200)	Scint	Coarse	41.78	±0.40	100	100
Cu	Kα	LiF(200)	Scint	Coarse	45.01	±0.40	100	100
Ni	Kα	LiF(200)	Scint	Coarse	48.67	±0.60	100	100
Cr	Kα	LiF(200)	FPC	Fine	69.36	±0.50	100	100
Fe	Kα	LiF(220)	FPC	Fine	85.71	–0.40+0.70	40	40
V	Kα	LiF(220)	FPC	Fine	123.00	–0.50	100	100
TiO_2	Kα	LiF(200)	FPC	Fine	86.11	±0.50	40	40
Ce	Lα	LiF(220)	FPC	Coarse	128.16	±1.50	100	100
Ba	Lβ	LiF(220)	FPC	Coarse	128.75	±1.50	100	100

FPC = flow proportional counter using P_{10} gas; Scint = NaI scintillation counter. Elements analyzed under vacuum using goniometer 1 at generator settings of 60 kV and 50 mA.

Table 2. Replicate XRF analyses of standard DRN during Leg 145.

	Run 1	Run 2	Run 3	Reference
Nb	7	7	8	8
Zr	128	132	125	125
Y	26	25	27	28
Sr	401	397	401	400
Rb	74	72	74	73
Zn	179	179	178	145
Cu	50	49	51	50
Ni	18	17	16	15
Cr	36	35	37	42
V	230	222	233	220
Ba	377	371	378	385
TiO_2	1.09%	1.10%	1.10%	1.09%

conversion was typically straightforward, involving extrapolation of the placement of a datum within an individual magnetic polarity chron. The correlation of the geologic epochs and periods used followed those of Berggren, Kent, and Flynn (1985) and Berggren, Kent, and Van Couvering (1985), with the exception of the Miocene/Pliocene boundary, where the calibration of Zijderveld et al. (1986) was used.

Figure 11 shows correlation of the diatom, radiolarian, and calcareous nannofossil zones to the geomagnetic polarity time scale of Cande and Kent (1992) for the Neogene.

In the following sections for calcareous nannofossils, radiolarians, and diatoms, ages of biostratigraphically useful datums have been given for the Berggren, Kent, and Flynn (1985); Berggren, Kent, and Van Couvering (1985); and Cande and Kent (1992) geomagnetic polarity time scales. The source of correlation of the individual datums to the magnetic polarity chrons also is given.

Foraminifers

Sample Preparation

Approximately 10 cm^3 of sediment was taken from each core-catcher sample. These samples were then disaggregated in a Calgon™ solution and washed with tap water through a 63-µm sieve. Samples that were difficult to disaggregate were pre-treated with a 3% hydrogen peroxide solution. Residues were sieved, and the >150-µm-size fraction was examined for planktonic and benthic foraminifers.

Planktonic foraminiferal abundance was defined as follows:

R = Rare (<10 specimens),
F = Few (10–100 specimens),
C = Common (100–500 specimens), and
A = Abundant (>500 specimens).

Benthic foraminiferal abundance was defined as follows:

R = Rare (<10 specimens),
C = Common (10–100 specimens), and
A = Abundant (>100 specimens).

Three classes of foraminiferal preservation were used:

P = Poor (almost all specimens were fragmented and showed evidence of dissolution and/or recrystallization),

M = Moderate (30%–90% of the specimens were fragmented or showed evidence of dissolution and/or recrystallization), and

G = Good (>90% of the specimens were unbroken and well preserved).

Paleoenvironmental Analysis

Benthic foraminifers were used primarily as paleoenvironmental indicators of paleodepth. Benthic foraminifers were examined from the >150-µm-size fraction. Paleobathymetric estimates were based primarily on van Morkhoven et al.'s (1986) depth zonations. Bathymetric ranges are as follows: neritic (0–200 m), upper bathyal (200–600 m), middle bathyal (600–1000 m), lower bathyal (1000–2000 m), and abyssal (>2000 m).

Calcareous Nannofossils

Chronological Framework

Age estimates of Cenozoic calcareous nannofossil zonal boundaries, or marker events (Table 3), have largely been derived from the geomagnetic polarity time scales (GPTS) of Berggren, Kent, and Flynn (1985) and Berggren, Kent, and Van Couvering (1985). Their polarity history covers the time interval from the present to 84 Ma (termination of Chron 34). For Leg 145, these age estimates were revised using the new GPTS by Cande and Kent (1992). These revised age estimates are also shown in Table 3. The GPTS of Kent and Gradstein (1985) has been used in the Cretaceous time interval older than Chron 34. This particular event in time connects the two time scales.

The progressively increasing availability of Cenozoic biomagnetostratigraphies in deep-sea sediments has resulted in steadily improved correlations between nannofossil biostratigraphy and the geomagnetic polarity history, improvements that are accounted for in Table 3.

The biochronology of Cretaceous calcareous nannofossil marker events still lacks much of the detail that exists for Cenozoic markers,

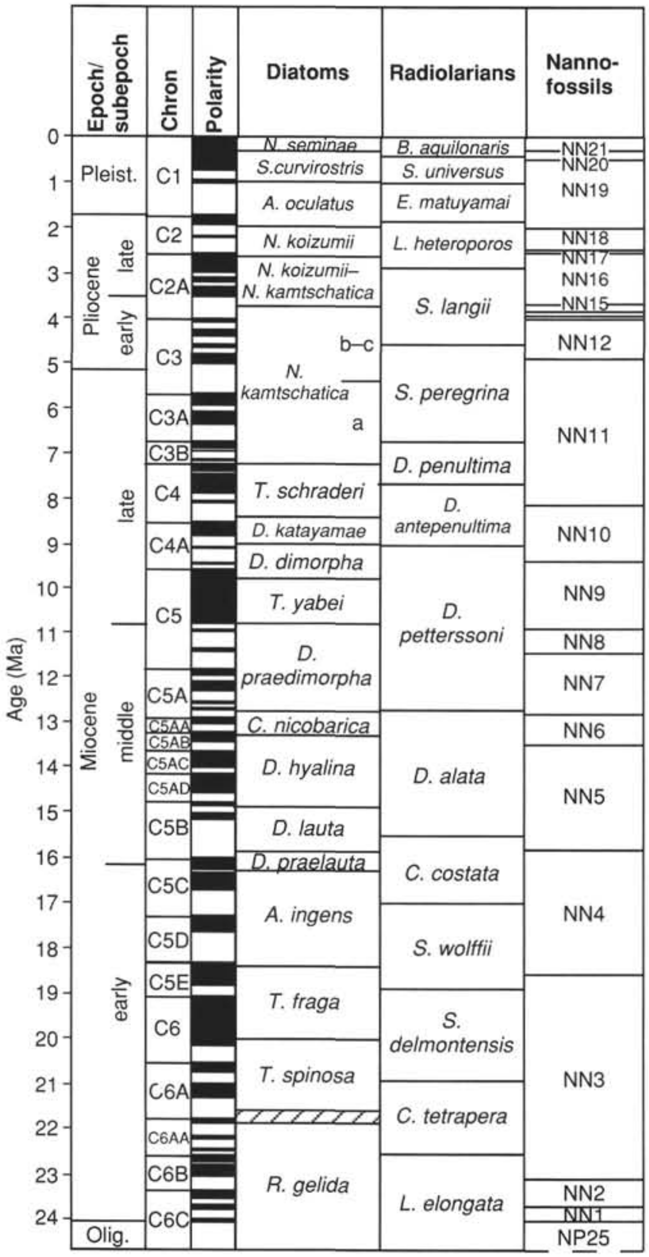

Figure 11. Correlation of diatom, radiolarian, and calcareous nannofossil zones used during Leg 145 (see text) to the geomagnetic polarity time scale of Cande and Kent (1992).

simply because the number of direct correlations between biostratigraphy and magnetostratigraphy are fewer in the Cretaceous. For this reason we have listed age assignments only for Cenozoic marker events.

Cenozoic Zonation

From a number of zonal schemes available for nannofossil subdivision of Cenozoic sediments, the scheme of Martini (1971) was chosen. This scheme does not represent the ultimate resolution (e.g., the number of evolutionary appearances/disappearances per unit time) that can be achieved in Cenozoic deep-sea sediments, because deep-sea biostratigraphy has developed rapidly over the past two decades and continues to do so. Yet, this zonal scheme provides a simple picture of biostratigraphic relationships in the cored sequences. The fact that most marine geologists are familiar with Martini's scheme also adds to its value as an initial framework for Leg 145 nannofossil biostratigraphy.

We have, however, also used numerous biostratigraphic events that were not used in Martini's (1971) zonal boundary definitions (Table 3). Hence, these additional events represent a resource that creates an improved biostratigraphic and biochronologic resolution, which becomes important, for example, in the reconstruction of Cenozoic sediment accumulation rates.

Cretaceous Zonation

The zonations of Sissingh (1977) and Thierstein (1976), together with those of Berggren, Kent, and Flynn (1985) and Berggren, Kent, and Van Couvering (1985), were used from the K/T boundary to the termination of Chron 34. The zonations of Sissingh (1977) and Thierstein (1976), as well as Kent and Gradstein's (1985) GPTS, were used from there and beyond.

Methods

Smear slides were prepared for each sample, using Ayac as a mounting medium. The calcareous nannofossils were examined in smear slides by standard light microscopy techniques (plane-polarized light, phase-contrast, or cross-polarized light at approximately 790×, or 1250×, magnification).

Calcareous nannofossils often show signs of both strong etching and strong overgrowth; more dissolution-resistant forms add secondary calcite provided by more dissolution-prone morphotypes. We have adopted a simple code system for characterizing preservational states. Preservation was recorded using one of the three following letter designations:

G = Good; little or no evidence of dissolution and/or secondary overgrowth of calcite, diagnostic features fully preserved.

M = Moderate; dissolution and/or secondary overgrowth partially alter primary morphological characteristics, but nearly all specimens can be identified at the species level.

P = Poor; severe dissolution, fragmentation, and/or secondary calcite overgrowth with primary features largely destroyed; many specimens cannot be identified at the species or generic level.

Estimates of abundances of the nannofossils in the smear slides were done using optimum density areas of the slide; that is, areas where most of the field was covered with sample material without appreciable piling of specimens or sample material. Four different levels of relative abundances, similar to the format outlined by Hays (1970), are defined as follows:

A = Abundant: >10% (usually more than 10 specimens per field of view).

C = Common: 1%–10% (1 to 10 specimens per field of view).

F = Few: 0.1%–1% (1 specimen per 1 to 10 fields of view).

R = Rare: <0.1% (only 1 specimen in more than 10 fields of view).

Radiolarians

Zonation

The radiolarian zonation (Fig. 11) for Pliocene and Pleistocene North Pacific Ocean sediments was constructed from the work of Hays (1970), Foreman (1975), and Morley (1985). For North Pacific sediments older than late Miocene, several studies (Sakai, 1980; Morley, 1985) have applied the low-latitude radiolarian zonation developed by Riedel and Sanfilippo (1970, 1971, 1978). All Miocene sediments analyzed in these previous reports, however, came from sites south of 44°N. Therefore, the radiolarian zonation for Miocene and older sediment sequences was chosen as a working model to be revised with information collected during this leg of the Ocean Drilling Program. Table 4 lists selected radiolarian species events which, based on their presence, will be applied to North Pacific Cenozoic sediments, with ages based on the Berggren, Kent, Flynn (1985) and Berggren, Kent, and Van Couvering (1985) and Cande and Kent (1992) geomagnetic time scales.

Methods

Preparation of radiolarian samples for microscopic examination during Leg 145 followed the methods described by Sanfilippo et al. (1985). Between 3 and 5 cm^3 of sediment was disaggregated and oxidized in a 10% hydrogen peroxide solution. In addition, those samples containing carbonate were treated with a 10% solution of hydrochloric acid to dissolve all calcareous microfossils. Oligocene and older samples were treated as described above (with hydrogen peroxide and hydrochloric acid), but heated to boiling to accelerate the deflocculation of clays. Brief treatment of most samples in an ultrasonic bath was followed by washing in a 63-µm mesh sieve. Strewn slides were prepared from the residue for examination of radiolarians.

Abundance and preservation of radiolarians were assessed qualitatively. Radiolarian assemblage abundance was assessed as follows:

A = Abundant (>500 specimens on slide [22 × 50 mm]),
C = Common (100–500 specimens on slide),
F = Few (50–100 specimens on slide), and
R = Rare (<50 specimens on slide).

Preservation of the radiolarian assemblage was based on the following criteria:

1. Good = Radiolarians show little sign of dissolution with only minor fragmentation.
2. Moderate = Radiolarians show evidence of moderate dissolution with obvious fragmentation.
3. Poor = Radiolarians show signs of a high degree of dissolution with few intact specimens.

Diatoms

Zonation

The diatom zonation used (Fig. 12) for the Neogene closely follows the zonation of Akiba (1985) with two changes: (1) the LO of *Neodenticula koizumii* is used to define the base of the *Actinocyclus oculatus* Zone, as is suggested by Koizumi (1992), and (2) the *Neodenticula kamtschatica* Zone is used in its traditional sense, as the interval from the FO of *N. kamtschatica s.str.* to the FO of *N. koizumii*. The *N. kamtschatica* Zone is divided into subzone a and subzone interval b-c by the FO of *T. oestrupii*, as was proposed by Barron (1980). A third modification to the Akiba (1985) zonation uses the LO of *Rocella gelida* as the marker species for the base of the *Thalassiosira spinosa* Zone, rather than the FO of *T. spinosa*, based on F. Akiba's observation (pers. comm., 1992) of the scarcity of *T. spinosa* in lowermost Miocene sediments from Japan.

Datum Levels

Table 5 lists absolute age estimates for Neogene and Oligocene diatom datum levels that have been found to be useful in the North Pacific Ocean. Ages are presented according to both Berggren, Kent, and Flynn's (1985); Berggren, Kent, and Van Couvering's (1985); as well as Cande and Kent's (1992) geomagnetic polarity time scales.

Methods

Strewn slides were prepared by placing a small amount of material in a snap-cap vial, adding distilled water, agitating the vial, and removing part of the upper suspension with a pipette. When required (because of a low concentration of diatoms or an induration of the sediment), selected samples were processed by boiling them in hydrogen peroxide and hydrochloric acid, then using the centrifuge (at 1200 rpm for 2–4 min) to remove these chemicals from the suspension. Strewn slides were examined in their entirety at 500× for stratigraphic markers and paleonvironmentally sensitive taxa. Identifications were checked routinely at 1250×. These abundances were recorded as follows:

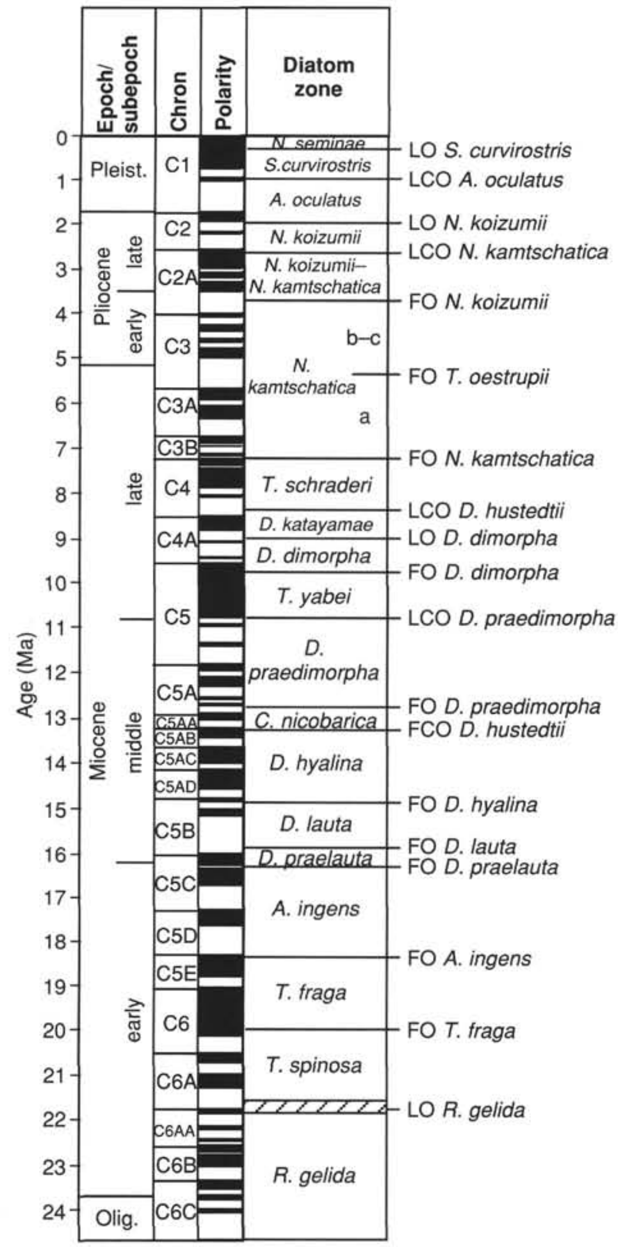

Figure 12. Correlation of Neogene diatom zonation used for Leg 145 (modified from Akiba, 1985, and Koizumi, 1992) to the geomagnetic polarity time scale of Cande and Kent (1992). LO = last occurrence; LCO = last common occurrence; FO = first occurrence; FCO = first common occurrence.

A (abundant) = Two or more specimens per field of view;
C (common) = One specimen per two fields of view;
F (few) = One specimen per each vertical traverse; and
R (rare) = < for sparser occurrences.

Preservation of diatoms was determined qualitatively as follows:

G (good) = finely silicified forms were present and no alteration of frustules was observed;

Table 3. Ages of biostratigraphically useful Cenozoic calcareous nannofossil datum levels calibrated to the Berggren et al. (1985) and Cande and Kent (1992) geomagnetic polarity time scales.

	Event	Zone (Top)	Age[a] (Ma)	Ageb (Ma)	Reference
OA	*Emiliania huxleyi*		(0.085)	0.091	1
FO	*Emiliania huxleyi*	NN20	(0.275)	0.294	1
LO	*Pseudoemiliania lacunosa*	NN19	(0.461)	0.493	1
LO	small *Gephyrocapsa*				
FO	*Gephyrocapsa* sp.3		(0.92)	0.99	2
FO	small *Gephyrocapsa*				
LO	*Gephyrocapsa* >5µm		(1.12)	1.19	2
FO	*Gephyrocapsa* >5µm		(1.32)	1.40	2
LO	*Calcidiscus macintyrei*		(1.45)	1.54	3
FO	*Gephyrocapsa oceanica* s.l.		(1.58)	1.67	2
LO	*Discoaster brouweri*	NN18	(1.89)	2.00	3
OA	*Discoaster triradiatus*		(2.07)	2.19	5
LO	*Discoaster pentaradiatus*	NN17	(2.35)	2.47	3
LO	*Discoaster surculus*	NN16	(2.41)	2.54	3
LO	*Discoaster tamalis*		(2.65)	2.78	3
LO	*Sphenolithus* spp.		(3.45)	3.60	3
LO	*Reticulofenestra pseudoumbilica*	NN15	(3.56)	3.71	3
LO	*Amaurolithus tricorniculatus*	NN14	(3.70)	3.85	6a
FO	*Discoaster asymmetricus*	NN13	(3.83)	3.98	4
LO	*Amaurolithus primus*		(4.37)	4.58	9
LO	*Ceratolithus acutus*		(4.43)	4.65	9
FO	*Ceratolithus rugosus*	NN12	(4.66)	4.92	9
FO	*Ceratolithus acutus*		(5.33)	5.68	9
FO	*Amaurolithus amplificus*		(6.02)	6.48	9
FO	*Amaurolithus primus*		(6.42)	6.80	14
FO	*Discoaster quinqueramus*	NN10	(7.46)	8.12	7
FO	*Discoaster berggrenii*		(7.50)	8.16	14
LO	*Discoaster hamatus*	NN9	(8.67)	9.37	7
LO	*Catinaster* spp.		(8.77)	9.47	7
FO	*Discoaster neohamatus*		(8.96)	9.62	7
LO	*Coccolithus miopelagicus*		(9.94)	10.4	14
FO	*Catinaster calyculus*		(10.0)	10.5	6a
FO	*Discoaster hamatus*	NN8	(10.5)	10.9	7
FO	*Catinaster coalitus*	NN7	(11.1)	11.4	7
LO	*Cyclicargolithus floridanus*		(11.5)	11.8	13
FO	*Discoaster kugleri*	NN6	(12.7)	12.8	13
LO	*Coronocyclus nitescens*		(12.8)	12.9	9
TC	*Cyclicargolithus floridanus*		(13.1)	13.2	7
LO	*Sphenolithus heteromorphus*	NN5	(13.5)	13.5	13
LO	*Helicosphaera ampliaperta*	NN4	(16.0)	15.8	6a
TA	*Discoaster deflandrei* group		(16.05)	15.9	9
FO	*Sphenolithus heteromorphus*		(18.42)	18.2	7
LO	*Sphenolithus belemnos*	NN3	(18.8)	18.5	7
FO	*Sphenolithus belemnos*		(19.46)	19.2	13
LO	*Triquetrorhabdulus carinatus*	NN2	(23.0)	23.1	13
FO	*Discoaster druggii*	NN1	(23.6)	23.7	7
TA	*Sphenolithus delphix*		(23.6)	23.7	10
LO	*Reticulofenestra bisecta*	NP25	(23.8)	23.8	6a
OA	*Sphenolithus delphix*		(24.7)	24.3	10
LO	*Sphenolithus ciperoensis*		(25.2)	24.6	7
OA	*Triquetrorhabdulus carinatus*		(27.0)	26.0	10
LO	*Sphenolithus distentus*	NP24	(27.5)	26.3	10
AS	*S. ciperoensis/S. distetntus*		(28.8)	28.3	10
FO	*Sphenolithus ciperoensis*	NP23	(30.2)	28.6	6b
FO	*Sphenolithus distentus*		(34.2)	32.1	6b
LO	*Reticulofenestra umbilica* (>14 µm)	NP22	(33.8)	31.7	11
LO	*Ericsonia formosa*	NP21	(34.9)	32.7	11
LO	*Discoaster saipanensis*	NP19-20	(37.7)	35.0	11
LO	*Discoaster barbadiensis*		(37.7)	35.0	11
FO	*Isthmolithus recurvus*	NP18	(37.8)	35.1	6b
FO	*Chiasmolithus oamaruensis*	NP17	(39.8)	36.9	6b
LO	*Chiasmolithus grandis*		(40.0)	39.7	6b
LO	*Chiasmolithus solitus*	NP15-16	(42.3)	39.7	6b
FO	*Reticulofenestra hesslandii*		(42.9)	40.4	11
LO	*Nannotetrina* spp.		(44.2)	41.9	11
FO	*Reticulofenestra umbilica* (>14 µm)		(44.4)	42.2	11
LO	*Chiasmolithus gigas*		(47.0)	44.6	6b
FO	*Chiasmolithus gigas*		(48.8)	46.3	12
FO	*Nannotetrina fulgens*	NP14	(49.5)	47.0	12
LO	*Discoaster sublodoensis*		(49.7)	47.2	12
FO	*Nannotetrina* spp.		(50.3)	47.8	12
LO	*Discoaster lodoensis*		(50.4)	47.9	12
FO	*Discoaster sublodoensis*	NP13	(52.3)	49.3	12
LO	*Tribrachiatus orthostylus*	NP12	(54.0)	50.8	12
FO	*Discoaster lodoensis*	NP11	(55.0)	52.0	12
FO	*Sphenolithus radians*		(56.0)	53.2	12
AS	*T. orthostylus/T. contortus*	NP10	(56.2)	53.3	12
FO	*Tribrachiatus contortus*		(56.5)	53.6	12
FO	*Tribrachiatus bramlettei*	NP9	(56.7)	53.9	12
FO	*Discoaster diastypus*		(56.7)	53.9	12
FO	*Rhomboaster* spp.		(56.8)	54.0	12
LO	*Fasciculithus* spp.		(56.9)	54.1	12

Table 3 (continued).

	Event	Zone (Top)	Age[a] (Ma)	Age[b] (Ma)	Reference
LO	*Ericsonia robusta*		(57.8)	55.1	12
FO	*Campylosphaera eodela*		(58.2)	55.5	6b
FO	*Discoaster multiradians*	NP8	(59.0)	56.3	12
FO	*Discoaster okadai*		(59.3)	56.6	12
FO	*Discoaster nobilis*		(59.4)	56.7	12
LO	*Heliolithus kleinpelli*		(60.1)	57.7	12
FO	*Discoaster mohleri*	NP6	(60.2)	57.8	12
LO	*Chiasmolithus danicus*		(61.0)	58.6	6b
FO	*Heliolithus kleinpelli*	NP5	(61.0)	58.6	12
FO	*Heliolithus cantabriae*		(61.5)	59.3	12
LO	*Fasciculithus pileatus*		(61.8)	59.7	12
LO	*Cruciplacolithus tenuis*		(61.8)	59.7	6b
FO	*Fasciculithus* spp.		(62.4)	60.6	12
FO	*Ellipsolithus macellus*	NP3	(62.8)	61.2	12
FO	*Sphenolithus* spp.		(62.9)	61.4	12
FO	*Chiasmolithus danicus*	NP2	(64.8)	64.1	6b
FO	*Cruciplacolithus tenuis*	NP1	(65.9)	65.4	6b
FO	*Cruciplacolithus primus*		(66.1)	65.6	6b

[a] Age estimates found by using the time scale of Berggren et al. (1985).
[b] Age estimates found by using the time scale of Cande and Kent (1992).

Notes: FO = first occurrence; LO = last occurrence; OA = onset acme; TA = termination acme; AS = abundance shift; TC = termination of continuous presence. Zonal codes are those of Martini (1971). Age column references represent: (1) Thierstein et al., 1977; (2) Rio et al., in press; (3) Backman and Shackleton, 1983; (4) Rio et al., 1991a; (5) Backman and Pestiaux, 1986; (6a) Berggren, Kent, and Flynn, 1985; (6b) Berggren, Kent, and Van Couvering, 1985; (7) Backman et al., 1990; (8) Zijderveld et al., 1986; (9) Rio et al., 1990b; (10) Fornaciari et al., 1990; (11) Backman, 1987; (12) Backman, 1986; (13) Olafsson, 1991; Shipboard Scientific Party, 1992.

Martini (1971) defined the top of Zone NP10 by the LO of *T. contortus*. Proneness to diagenetic overgrowth in combination with a subtle evolutionary transition into the descendant species *T. orthostylus* prevents precise determination of the NP10/NP11 boundary. The abundance crossover between these closely related forms, however, provides a biostratigraphic indication that is easier to recognize than the LO of *T. contortus*.

M (moderate) = finely silicified forms were present, but they exhibited some alteration; and

P (poor) = finely silicified forms are absent or rare and fragmented, and the assemblage is dominated by robust forms.

PALEOMAGNETISM

Laboratory Facilities

The Paleomagnetism Laboratory aboard the *JOIDES Resolution* is equipped with two magnetometers: (1) a pass-through cryogenic superconducting rock magnetometer manufactured by 2-G Enterprises (Model 760R) and (2) a Molspin spinner magnetometer. For Leg 145, the Japanese automatic ring-core fluxgate spinner magnetometer (designed by N. Niitsuma) was also brought on board the ship. The laboratory has an alternating field (AF) demagnetizer and a thermal demagnetizer (Models GSD-1 and TSD-1 by the Schonstedt Instrument Co.) capable of demagnetizing discrete specimens to 100 mT and 700°C, respectively. In addition, an in-line AF demagnetizer, capable of 25 mT (2-G Model 2G600), is included on the pass-through cryogenic magnetometer track for demagnetization of whole-core sections.

The sensing coils in the cryogenic magnetometer measure signals over about a 20-cm interval, and the coils for each axis have slightly different response curves. The widths of the sensing regions correspond to about 200–300 cm^3 volume of cored material, which contributes to the signal at the sensors. The large volume of core material within the sensing region permits accurate determination of the remanence for weakly magnetized samples, despite the relatively high background noise related to the motion of the ship. In fact, the practical limit on the sensitivity may be imposed by the magnetization of the core liner itself (about 0.1 mA/m = 10^{-7}emu/cm^3).

The pass-through cryogenic magnetometer and its AF demagnetizer interface with an IBM PC-AT-compatible computer and are controlled by a BASIC software program modified from the original SUPERMAG program. We noted that the current version of the SUPERMAG program was previously modified to compensate for end effects. To do so, the program divides the sensor output by the portion of the area under the response curves contained in the sediment. The spinner magnetometer, used for measuring discrete samples, interfaces with a Macintosh SE/30 through a program brought on board the ship by D. Schneider (WHOI) for Leg 138.

The Japanese spinner automatically demagnetizes and measures samples having AF fields up to 45 mT. The instrument is also capable of measuring susceptibility and susceptibility anisotropy and of inducing ARM magnetizations.

The magnetic susceptibility of unsplit sections of core was measured with Bartington Instruments's Model MS1 susceptibility meter adapted with a MS1/CX 80-mm whole-core sensor loop set at 0.465 kHz. The full width of the impulse response peak at half maximum is less than 5 cm. The susceptibility sensor is mounted with the GRAPE and P-wave logger on the multisensor track (MST). The susceptibility of discrete specimens can be measured on board the ship with a sensor unit (Type MS1B) attached to the Bartington susceptibility meter.

Paleomagnetic Measurements

Pass-through Magnetometer

The bulk of the paleomagnetic measurements on Leg 145 was performed with the pass-through cryogenic magnetometer. Pass-through paleomagnetic measurements were routinely performed on the archive halves of the 1.5-m core sections. The ODP core orientation scheme arbitrarily designates the *X*-axis as the horizontal (in situ) axis radiating from the center of the core through the space between a double line scribed lengthwise on the working half of each core liner. Natural remanent magnetizations (NRM) and remanences after the 10 and/or 15 mT AF demagnetization were routinely measured at 5-cm intervals. Occasionally, the measuring interval of the NRM and, more rarely, the demagnetized remanence was increased to 10 cm. This was done when the magnetic signal was very weak and it was apparent that the magnetic polarity could not be resolved, or to accelerate core flow through the laboratory.

The NRM was generally dominated by a vertical upward magnetization, presumably acquired during coring. Still, the NRM measurements contain important information about the expected magnetization of the sediment and possibly the origin of the overprinting. The

Table 4. Ages of Neogene radiolarian datum levels based on the Berggren et al. and Cande and Kent geomagnetic polarity time scales.

	Datum	Berggren et al.[a] (Ma)	CK92[b] (Ma)	Reference
LO	*Lychnocanoma grande*	0.05	0.05	1
LO	*Druppatractus acquilonius*	0.33	0.35	1
LO	*Stylatractus universus*	0.425	0.45	2
LO	*Lamprocyrtis neoheteroporos*	0.73	0.78	3
LO	*Eucyrtidium matuyamai*	0.98	1.05	3
LO	*Lamprocyrtis heteroporos*	1.0	1.07	3
LO	*Pterocanium prismatium*	1.6	1.7	4
FO	*Eucyrtidium matuyamai*	1.8	1.9	3
FO	*Cycladophora davisiana*	2.7	2.8	5
LO	*Stichocorys peregrina*	2.8	2.9	3
FO	*Lamprocyrtis neoheteroporos*	2.9	3.0	4
LO	*Phormostichoartus fistula*	3.25	3.4	6
LO	*Stichocorys delmontensis*	3.4	3.55	3
LO	*Botrystrobus bramlettei*	4.15	4.3	6
FO	*Lamprocyrtis heteroporos*	4.4	4.6	5
LO	*Lychnocanoma nipponica nipponica*	4.4	4.6	9
FO	*Sphaeropyle langii*	4.4	4.6	3
FO	*Botryostrobus aquilonaris*	6.2	6.6	6
FO	*Druppatractus acquilonius*	6.4	6.75	11
FCO	*Stichocorys peregrina*	6.4	6.75	7
LO	*Didyomocyrtis penultima*	6.7	7.25	5
LO	*Diartus hughesi*	6.9	7.5	6
FO	*Stichocorys peregrina*	7.0	7.6	10
LO	*Lynchnocanoma nipponica magnacornuta*	7.9	8.5	11
FO	*Didymocyrtis penultima*	8.4	9.1	5
FO	*Diartus hughesi*	8.75	9.5	6
FO	*Botryostrobus bramlettei*	10.05	10.5	6
FO	*Didymocyrtis antepenultima*	10.8	11.2	5
LO	*Cyrtocapsella japonica*	10.8	11.2	5
LO	*Diartus petterssoni*	11.1	11.4	5
LO	*Stichocorys wolffii*	11.6	11.9	8
LO	*Cyrtocapsella cornuta*	11.6	11.9	
LO	*Cyrtocapsella tetrapera*	11.8	12.1	5
FO	*Lynchnocanoma nipponica magnacornuta*	11.9	12.15	11
LO	*Eucyrtidium inflatum*	11.95	12.2	11
LO	*Eucytrtidium asanoi*	12.6	12.7	9
FO	*Diartus petterssoni*	12.6	12.7	6
FO	*Lychnocanoma nipponica nipponica*	14.25	14.2	9
FO	*Eucyrtidium inflatum*	14.9	14.8	11
LO	*Calocycletta costata*	15.0	14.9	7
FO	*Eucytrtidium asanoi*	15.2	15.1	9
FO	*Dorcadospyris alata*	15.7	15.5	8
LO	*Dorcadospyris dentata*	15.8	15.6	8
LO	*Lychnocanoma elongata*	16.5	16.3	8
FO	*Dordacospyris dentata*	17.1	17.0	8
FO	*Calocycletta costata*	17.3	17.1	8
FO	*Stichocorys wolffii*	19.2	18.9	7
FCO	*Didymocyrtis violina*	19.25	19.0	8
LO	*Theocyrtis annosa*	21.0	20.6	7
LO	*Artophomis gracillis*	22.5	22.5	8
FO	*Cyrtocapsella tetrapera*	22.6	22.6	7
FO	*Prunopyle titan*	22.6	22.6	
FO	*Lychnocanoma elongata*	25.9	25.1	8

[a] Berggren, Kent, and Flynn (1985) and Berggren, Kent, and Van Couvering (1985).

Notes: LO = last occurrence; FO = first occurrence; FCO = first common occurrence. Sources for ages of datum levels: (1) Morley et al., 1992; (2) Hays and Shackleton, 1976; (3) Morley, 1985; (4) Johnson et al., 1989; (5) Spencer-Cervato elt al., in press; (6) Johnson and Nigrini, 1985; (7) Shipboard Scientific Party, 1992; (8) Nigrini, 1985; (9) Sakai, 1980; (10) Weaver et al., 1981; (11) new calibration from Sites 884 and 887.

magnetostratigraphic interpretations for Leg 145 are based on the pass-through measurements of the demagnetized cores, checked by results from discrete specimens measured using either spinner magnetometer. Data from core segments that are clearly physically disturbed, sometimes up to 50 cm from core tops, have been deleted from the data files. Other segments of core, which are magnetically noisy and uninterpretable or have an insufficient magnetic signal, were excluded from shipboard analysis, but the data are retained in the primary ODP data files.

Low-field Susceptibility

Whole-core susceptibility measurements are relatively rapid to make, nondestructive, and provide an indication of the amount of magnetizable material in the sediment, including ferrimagnetic and paramagnetic constituents. Whole-core volume magnetic susceptibility was measured using the automated MST. Measurements were performed at the low sensitivity range (1.0) and in the SI mode, usually every 5 cm, depending on the available time for shipboard measurements. When the susceptibility decreased to a level indistinguishable from instrumental noise, the measurement interval was increased to 15 or 20 cm. The susceptibility data were archived in raw instrument meter readings. To convert these values to susceptibility units, one must multiply by 0.63, calculated from the manufacturer's manual, to compensate for the 0.77 ratio of core diameter (68 mm) to coil diameter (88 mm). An additional multiplicative factor of 10^{-5} is necessary to complete the conversion to volume normalized SI. These factors were checked against the values expected for distilled water. The meter was zeroed with each section, but no shipboard correction was made for instrumental baseline-drift of each 1.5-m susceptibility

Table 5. Ages of biostratigraphically useful Neogene and Oligocene diatom datum levels calibrated to the Berggren et al. (1985) and Cande and Kent (1992) geomagnetic polarity time scales.

	Datum	Berggren et al.[a] (Ma)	CK92[b] (Ma)	Paleomagnetism	References
LO	*Simonseniella curvirostris*	0.3	0.3	C1n.1n	3
LO	*Thalassiosira jouseae*	0.39–0.28	0.41–0.30	C1n.1n	1
LO	*Rhizosolenia matuyamai*	0.97–0.85	1.04–0.91	C1n.2n	1
FO	*Rhizosolenia matuyamai*	1.05–0.91	1.12–0.98	C1n.2n	1
LCO	*Actinocyclus oculatus*	1.33–0.93	F1.44–1.00	C1n.2n	
FO	*Simonseniella curvirostris*	1.5	1.58	C1r.2r	1
LO	*Coscinodiscus pustulatus*	1.7	1.8		4
LO	*Pyxidicula horridus*	1.7	1.8		2
LO	*Thalassiosira antiqua*	1.7–1.43	1.8–1.5		1
LO	*Neodenticula koizumii*	1.9	2.0	C2r.1r	3
LO	*Pyxidicula zabelinae*	2.0	2.1		2
LO	*Thalassiosira convexa*	2.3	2.4		2
LCO	*Neodenticula kamtschatica*	2.5–2.58	2.63–2.7	C2An.1n	1
FO	*Neodenticula seminae*	2.6	2.7		3
LO	*Thalassiosira jacksonii*	3.2	3.3		3
FO	*Neodenticula koizumii*	3.6	3.75	C2A.3r	1
FO	*Actinocyclus oculatus*	3.7	3.8		3
FO	*Thalassiosira latimarginata*	4.77	5.05	C3n.4n	9
FO	*Thalassiosira oestrupii*	5.1	5.4		2
LO	*Rouxia californica*	5.2	5.5		2
LO	*Thalassiosira miocenica*	5.35	5.7	C3An.1n	1
FO	*Thalassiosira praeoestrupii*	5.54	5.95	C3An.1r	8
LO	*Thalassiosira praeconvexa*	5.8	6.3	C3An.2n	2
FO	*Thalassiosira miocenica*	5.8	6.3	C3Ar.2n	2
FO	*Thalassiosira jacksonii*	6.4	6.8		1
FO	*Nitzschia reinholdii*	6.5	6.9		2
FO	*Neodenticula kamtschatica*	6.7	7.25	C4n.1n	9
LO	*Thalassionema schraderi*	6.8	7.45	C4n.1r	9
FO	*Thalassiosira antiqua*	7.6	8.3		2
LO	*Denticulopsis katayamae*	7.6	8.3		2
LCO	*Denticulopsis hustedtii*	7.8	8.4	C4r.3r	
LO	*Denticulopsis dimorpha*	8.4	9.0		2
FO	*Denticulosis katayamae*	8.7	9.3		2
FO	*Denticulopsis dimorpha*	9.2	9.8	C5n.1n	9
LCO	*Denticulopsis praedimorpha*	10.4	10.8	C5n.2n	
FO	*Simonseniella barboi*	11.2	11.5	C5r.3r	2
FO	*Hemidiscus cuneiformis*	11.4	11.7		2
FO	*Thalassiosira brunii*	11.5	11.8		2
LO	*Crucidenticula nicobarica*	12.2	12.4		2
FO	*Denticulopsis praedimorpha*	12.6	12.8	C5n.4n	5
LO	*Thalassiosira praeyabei*	13.4	13.4		2
FCO	*Denticulopsis hustedtii*	13.25	13.3	C5ABn	
FO	*Dentiuclopsis hustedtii*	14.3	14.2	C5An.8n	5
FO	*Thalassiosira praeyabei*	14.8	14.7		2
LO	*Crucidenticula kanayae*	14.8	14.7		2
FO	*Denticulopsis hyalina*	15.0	14.9	C5Br.1r	2
FO	*Actinocyclus ingens nodus*	15.2	15.1		2
LO	*Denticulopsis praelauta*	15.7–15.3	15.6–15.2		2
FO	*Denticulopsis lauta*	16.0	15.9		2
FO	*Denticulopsis praelauta*	16.3	16.2		2
LO	*Crucidenticula sawamurae*	18.6	18.4	C5En	9
FO	*Actinocyclus ingens*	18.6	18.4	C5En	9
FO	*Thalassiosira fraga*	20.4–20.3	20.1–20.0	C6r.1r	7
LO	*Rocella gelida*	22.1–21.8	21.9–21.6	C6AAn.1n	7
FO	*Thalassiosira spumellaroides*	22.6	22.6		6
FO	*Thalassiosira spinosa*	24.5–24.0	24.3–24.0		7
LO	*Lisitzinia ornata*	24.5	24.3	C6Cr.3r	6
LO	*Rocella vigilans*	26.3	25.4	C7r	6
FO	*Rocella gelida*	27.6–27.4	26.4–26.2	C8n.2n	7
FO	*Lisitzinia ornata*	29.2	27.9	C9r.2r	6
FO	*Rocella vigilans*	32.2	30.2	C11r.2r	6
LO	*Pyxilla reticulata*	32.3	30.3	C11r.2r	6
FO	*Synedra jouseana*	32.6	30.6	C12n.1n	6
LO	*Rhizosolenia oligocaenica*	33.4–33.3	31.1–31.0	C12r.1r	6
FO	*Rhizosolenia oligocaenica*	36.0–35.9	33.7–33.6	C13r.2r	7

[a] Berggren, Kent, and Flynn (1985); Berggren, Kent, and Van Couvering (1985).
[b] Cande and Kent (1992).

Notes: Sources for calibration: (1) Koizumi and Tanimura, 1985; (2) Barron, 1992; (3) Koizumi, 1992; (4) Barron, 1980; (5) Gersonde and Burckle, 1990; (6) Harwood and Maruyama, 1992; (7) Baldauf and Barron, 1991; (8) Bodén, in press; (9) new calibration from Site 884 magnetostratigraphy. LO = last occurrence; LCO = last common occurrence; FO = first occurrence; FCO = first common occurrence. Polarity chronology after Cande and Kent (1992).

profile, although the necessary parameters were recorded and will be processed at shore-based laboratories.

Core Orientation

Core orientation of the advanced hydraulic piston cores (APC) was achieved with an Eastman-Whipstock multishot tool and the new Tensor multishot tool, both of which are rigidly mounted onto the core barrel. The Eastman-Whipstock tool consists of a magnetic compass and a camera. The battery-operated camera photographs continuously at prescribed intervals from 0.5 to 2 min from the time it leaves the ship's deck. At the bottom of the hole, the core barrel is allowed to rest for sufficient time (2–8 min) to settle the compass needle and to make sure that several photographs are taken before the corer is shot into the sediment. (The photographs used for orientation are those taken just prior to shooting the core barrel into the sediment.).

The Tensor tool consists of three mutually perpendicular magnetic sensors and two perpendicular gravity sensors. The information from both sets of sensors allows the azimuth and dip of the hole to be measured as well as the azimuth of the APC core double orientation line.

Orientation is not usually attempted for the top three cores (about 30 m), until the bottom-hole assembly (BHA) is sufficiently stabilized in the sediment. Core orientation by the multishot tools was generally successful during Leg 145, with a subjective accuracy estimate of 20° to 30°, and contributed to the magnetostratigraphic interpretations. Exceptions to this typical performance are noted in the various site chapters (this volume).

Magnetostratigraphy

To maximize the chances for successful determination of the magnetostratigraphy and to satisfy the sampling needs of the shipboard paleomagnetists, who are interested in high-resolution studies of reversals and excursions, an effort was made to take most of the shipboard samples, including whole-round geochemical and physical properties samples, away from the reversal boundaries in the "B" holes. This was achieved using the whole-core magnetostratigraphy from the "A" (first-drilled) holes at each site to locate the reversal boundaries in the "B" (second-drilled) holes.

Whenever possible in the site chapters, we offer an interpretation of the magnetic polarity stratigraphy using the new magnetic polarity time scale of Cande and Kent (1992) (see Table 6). Two additional short geomagnetic features, observed with sufficient regularity that they may make useful stratigraphic markers for regional/global correlations, are the Blake feature at about 0.11 Ma in the Brunhes and the Cobb Mountain event at about 1.1 Ma. For the upper part of the time scale (roughly Pliocene-Pleistocene), we use the traditional names to refer to various chrons and subchrons (e.g., Gauss, Jaramillo). For older sediments, we follow the convention of using correlative anomaly numbers prefaced by the letter C. Normal polarity subchrons are referred to by adding suffixes (n1, n2), which increase with age. The reversal boundaries themselves are specified by the chron/subchron designation followed by the letter "o" (for onset) or "t" (for termination). Reverse polarity chrons or subchrons are similarly named with an R suffix (the reverse polarity portion of a chron being older than the corresponding normal polarity).

Table 6. Normal polarity intervals of the Cande and Kent (1992) magnetic reversal time scale used during Leg 145.

Normal polarity interval (Ma)	Polarity chron	Normal polarity interval (Ma)	Polarity chron
0.000–0.780	C1n	22.599–22.760	C6Bn.1n
0.984–1.049	C1r.1n	22.814–23.076	C6Bn.2n
1.757–1.983	C2n	23.357–23.537	C6Cn.1n
2.197–2.229	C2r.1n	23.678–23.800	C6Cn.2n
2.600–3.054	C2An.1n	23.997–24.115	C6Cn.3n
3.127–3.221	C2An.2n	24.722–24.772	C7n.1n
3.325–3.553	C2An.3n	24.826–25.171	C7n.2n
4.033–4.134	C3n.1n	25.482–25.633	C7An
4.265–4.432	C3n.2n	25.807–25.934	C8n.1n
4.611–4.694	C3n.3n	25.974–26.533	C8n.2n
4.812–5.046	C3n.4n	27.004–27.946	C9n
5.705–5.946	C3An.1n	28.255–28.484	C10n.1n
6.078–6.376	C3An.2n	28.550–28.716	C10n.2n
6.744–6.901	C3Bn	29.373–29.633	C11n.1n
6.946–6.981	C3Br.1n	29.737–30.071	C11n.2n
7.153–7.187	C3Br.2n	30.452–30.915	C12n
7.245–7.376	C4n.1n	33.050–33.543	C13n
7.464–7.892	C4n.2n	34.669–34.959	C15n
8.047–8.079	C4r.1n	35.368–35.554	C16n.1n
8.529–8.861	C4An	35.716–36.383	C16n.2n
9.069–9.149	C4Ar.1n	36.665–37.534	C17n.1n
9.428–9.491	C4Ar.2n	37.667–37.915	C17n.2n
9.592–9.735	C5n.1n	37.988–38.183	C17n.3n
9.777–10.834	C5n.2n	38.500–39.639	C18n.1n
10.940–10.989	C5r.1n	39.718–40.221	C18n.2n
11.378–11.434	C5r.2n	41.353–41.617	C19n
11.852–12.000	C5An.1n	42.629–43.868	C20n
12.108–12.333	C5An.2n	46.284–47.861	C21n
12.618–12.649	C5Ar.1n	48.947–49.603	C22n
12.718–12.764	C5Ar.2n	50.646–50.812	C23n.1n
12.941–13.094	C5AAn	50.913–51.609	C23n.2n
13.263–13.476	C5ABn	52.238–52.544	C24n.1n
13.674–14.059	C5ACn	52.641–52.685	C24n.2n
14.164–14.608	C5ADn	52.791–53.250	C24n.3n
14.800–14.890	C5Bn.1n	55.981–56.515	C25n
15.038–15.162	C5Bn.2n	57.800–58.197	C26n
16.035–16.318	C5Cn.1n	61.555–61.951	C27n
16.352–16.515	C5Cn.2n	63.303–64.542	C28n
16.583–16.755	C5Cn.3n	64.911–65.732	C29n
17.310–17.650	C5Dn	66.601–68.625	C30n
18.317–18.817	C5En	68.745–69.683	C31n
19.083–20.162	C6n	71.722–71.943	C32n.1n
20.546–20.752	C6An.1n	72.147–73.288	C32n.2n
21.021–21.343	C6An.2n	73.517–73.584	C32r.1n
21.787–21.877	C6AAn	73.781–78.781	C33n
22.166–22.263	C6AAr.1n	83.000–(118.0)	C34n
22.471–22.505	C6AAr.2n		

INORGANIC GEOCHEMISTRY

Interstitial-water Sampling and Chemistry

Shipboard interstitial-water analyses were performed on 5- to 10-cm-long whole-round sections that were cut immediately after the core arrived on deck. Samples were usually taken from each of the first six cores, from every second core down to about 170 mbsf, and from each third core thereafter. Advantage was taken of higher-resolution sampling where possible, such as in Hole 883A, where samples were collected from about every second core section. Interstitial waters were collected by applying pressure to the sediment using a titanium and stainless-steel squeezer (Manheim and Sayles, 1974). Before squeezing, whole-round surfaces were carefully scraped with teflon-coated spatulas to remove potentially contaminated exteriors. Whole-round sections were then placed into titanium cylinders atop a Whatman No. 1 filter paper round previously rinsed in high purity water to remove processing acids. A second filter paper round and a stainless-steel piston were placed on top of the sample in the cylinder and up to 40,000 lbs pressure (approximately 4150 psi) was applied with a hydraulic press. Interstitial water was expressed into a plastic syringe attached to the bottom of the assembly and filtered through a 0.45-μm Gelman polysulfone disposable filter. Samples were stored temporarily in plastic vials, pending analysis. Aliquots for future shore-based analyses were placed in acid-washed plastic tubes, acidified to ~pH 2 with concentrated HNO_3, and heat-sealed.

Interstitial-water samples were routinely analyzed for salinity as total dissolved solids using a Goldberg optical hand-held refractometer (Reichart); for pH and alkalinity by Gran titration with a Brinkmann pH electrode and a Metrohm autotitrator; for Cl, Ca, and Mg concentrations by titration; for SO_4 concentrations by ion chromatography with a Dionex 2120i chromatograph; and for Si, NO_2, and NH_4 concentrations by spectrophotometric methods using a Milton Roy Spectronic 301 spectrophotometer. The analytical techniques described by Gieskes et al. (1991) were followed throughout. International Association of Physical Sciences Organizations (IAPSO) standard seawater was used for calibrating most techniques. The reproducibility of these techniques, expressed as 1 sigma standard deviations of means of multiple determinations of IAPSO standard sea- water or of a standard, are alkalinity, 3%; Cl, 0.4%; Ca, <1%; Mg, 0.5%; SO_4, <2%; and Si, NO_2, and NH_4, 4%–5%.

K, Li, Sr, Mn, and Na (at Site 881 only) concentrations were quantified using flame spectrophotometric techniques with a Varian SpectrAA-20 atomic absorption unit. Na and K were determined in 1/500 diluted aliquots by flame emission using an air-acetylene flame with Cs as an ionization suppressant. Li and Sr were determined in 1/6 diluted aliquots. Li was determined by emission using an air-acetylene flame, and Sr by atomic absorption using an nitrous oxide-acetylene flame with La as a realizing agent. Mn was determined by atomic absorption in 1/5 diluted aliquots with added La. Standards for all flame spectrophotometric techniques were matched in matrix composition to the samples. The reproducibility of these techniques, expressed as 1 sigma standard deviations of means of multiple determinations of IAPSO standard seawater or of a standard treated as samples, are Na, <1–2%; K, <2–3%; Li, <1%–2%; Rb, <1%–2%; Sr, <2%; and Mn, 2%–3%. At all sites, Na was determined indirectly using charge balance calculations where $\sum$(cation charge) = $\sum$(anion charge). At Site 881, agreement with the sodium values (determined by atomic emission) was good.

Chemical data for interstitial waters are reported in molar units in each site report.

ORGANIC GEOCHEMISTRY

The shipboard organic geochemistry program for Leg 145 included (1) a real-time monitoring of the volatile hydrocarbons, as required by safety considerations, (2) measurement of inorganic carbon concentrations to determine the amount of carbonate in the sediments, (3) elemental analysis of total nitrogen, carbon and sulfur, and (4) determination of free hydrocarbons, pyrolyzable hydrocarbons, and maturity of organic matter. Detailed procedures are those described in Emeis and Kvenvolden (1986).

Hydrocarbon Gases

As required by safety considerations, the concentrations of the light hydrocarbons methane (C_1), ethane (C_2), and propane (C_3) were monitored in the sediment cores at intervals of approximately 10 m. Headspace samples were obtained by removing a 5-cm^3 plug of sediment from the end of a core as it arrived on deck, using a No. 6 cork borer (Kvenvolden and McDonald, 1986). The sample was placed immediately in a 21-mL glass vial that was sealed with a septum and metal crimp and then heated to 70°C for at least 30 min. The gas driven off was drawn into a syringe and analyzed.

The gas samples obtained were injected into a Hach-Carle AGC Series 100, Model 211 gas chromatograph equipped with a flame ionization detector and a 6 ft × 1/8 in. steel column packed with Porapak N:Q (80%/20%). The instrument has a detection limit for methane of 0.1 ppm. Details of this method and the complete configuration of the gas chromatograph are given in the "Explanatory Notes" chapter for Leg 112 (Shipboard Scientific Party, 1988).

Inorganic Carbon

Inorganic carbon was determined using a Coulometrics 5011 carbon dioxide coulometer equipped with a System 140 carbonate carbon analyzer. A known mass, ranging from 15 to 70 mg, of freeze-dried, ground, and weighed sediment was reacted in a 2N HCl solution. The liberated CO_2 was titrated in a monoethanolamine solution with a colorimetric indicator, while the change in light transmittance was monitored with a photo-detection cell. The percentage of carbonate was calculated from the inorganic carbon content, assuming that all carbonate occurs as calcium carbonate as follows:

$$CaCO_3 = IC\ (\text{inorganic carbon}) \cdot 8.334.$$

No corrections were done for siderite or dolomite.

Elemental Analysis

Total nitrogen, carbon, and sulfur of whole-rock samples were determined using an NCS analyzer, Model NA 1500 from Carlo Erba Instruments. Mixtures of vanadium pentoxide and crushed, freeze-dried samples were combusted in an oxygen atmosphere at 1000°C, converting organic and inorganic carbon to CO_2, sulfur to SO_2, and nitrogen to NO_2. The NO_2 was reduced to N_2 using copper. The gases were then separated by gas chromatography and measured with a thermal conductivity detector. Total organic carbon (TOC) was calculated by difference between total carbon (TC) from the NCS and inorganic carbon (IC) from the coulometer, as follows:

$$TOC = TC - IC.$$

PHYSICAL PROPERTIES

Shipboard measurements of physical properties help to define lithologic units, correlate lithology with downhole geophysical logs, and interpret seismic reflection and other geophysical data. The goal of the physical properties program of Leg 145, in addition to providing a link between lithologic and geophysical data, was to address some of the questions raised as a result of the extensive physical property analyses performed using the DSDP Leg 86 red clay samples and to complement a study of slope stability problems from continental margin settings.

Several types of measurements were performed in using the 1.5-m whole-round core sections. Continuous measurements of bulk density, compressional-wave velocity, and magnetic susceptibility were provided by the multisensor track (MST), while thermal conductivity measurements using the needle probe method were performed at discrete intervals.

Physical property measurements performed using samples obtained from the split cores included vane shear strength, compressional-wave velocity and attenuation, and index properties. Two intervals, within each section were sampled within the primary hole: one sample per section was sampled from additional holes.

Multisensor Track

The MST incorporates the gamma ray attenuation porosity evaluator (GRAPE), the P-wave logger (PWL), and a whole-core magnetic susceptibility device. Individual whole-core sections were placed horizontally on the MST core tray, which moves the section through the three sets of sensors. The MST produces a continuous record analogous to the in-situ record created by the borehole logging tools.

The GRAPE (bulk density) measurements were recorded at 1-cm intervals; the measurement is based on comparing the attenuation of gamma rays through the cores with the attenuation through an aluminum standard (Boyce, 1976). The GRAPE data are most reliable in APC cores. The presence of drilling slurry between XCB "biscuits" acts to lower the bulk-density values, and thus, GRAPE data in XCB cores can be used only as an indication of bulk-density trends and highs. The GRAPE record is useful for correlating among holes and sites. The PWL measures compressional wave velocity at 2-cm intervals. The transmitting and receiving transducers are aligned perpendicular to the core axis. A pair of displacement transducers monitors the separation between the compressional wave transducers; variations in the outside diameter of the liner therefore do not affect the accuracy of the velocity measurements. The transmitting transducer emits a 500-kHz compressional-wave pulse at a repetition rate of 1 kHz. Generally, only the APC cores were measured, as the XCB and RCB cores have voids between the core and the liner that result in transmission losses. Weak returns having signal strengths below a threshold value of 100 were removed.

The MST magnetic susceptibility procedures are included in the "Paleomagnetism" section, "Explanatory Notes" chapter (this volume).

Thermal Conductivity

The thermal conductivity measurement techniques used during Leg 145 are those described by Von Herzen and Maxwell (1959) and Vacquier (1985). Measurements were performed with a Thermcon-85 unit, and all data are reported in units of W/(m·°C). The estimated measurement error is about 5%–10%. All data were corrected for in-situ pressure and temperature (Ratcliffe, 1960), assuming hydrostatic pressure and a conductive thermal gradient of about 35°C/m.

To reduce background thermal transients, cores were allowed to equilibrate in their liners until the sediments reached a stable temperature (approximately 3–4 hr). Thermal conductivities were measured in Sections 2, 3, 4, and 5 of every soft-sediment core by inserting needle probes into the sediment through holes drilled through the liners. Sample temperatures were monitored with the thermistors in the probes, without applying a current to the heater wires. The measurement sequence was started once the background temperature drift was reduced to 0.04°C/min. Thermal conductivity was calculated from the rate of temperature increase in the probe while a heater current was flowing. The increase in temperature in the probe should vary logarithmically with time, as follows:

$$T(t) = (q/4\pi k) \ln(t) + \text{constant}, \qquad (1)$$

where k is the thermal conductivity, T and t are the temperature and time, respectively, and q is the heat generated per unit length of the probe. From Equation 1, the thermal conductivity is derived from the slope of temperature vs. the logarithm of time. Measurements of thermal conductivity were performed until the sediment became too lithified to insert the needle probes.

Vane Shear Strength

The undrained shear strength of the sediment was determined using the ODP motorized miniature vane shear device, following the procedures of Boyce (1977). The vane rotation rate was set to 89°/min. The vane used for all measurements has a 1:1 blade ratio with a blade dimension of approximately 1.27 cm.

The instrument measures the stress and strain at the vane shaft. The shear strength reported is calculated according to the vane size and spring torque factor (pre-calibrated) and the rotation of the stress pointer on the instrument. Both the undisturbed and the remolded strength were measured according to the procedure of Boyce (1977).

When analyzing vane tests one assumes that a cylinder of sediment is uniformly sheared about the axis of the vane in an undrained condition, with cohesion being the principal contributor to shear strength. Departures from this assumption include (1) progressive cracking within and outside of the failing specimen, (2) uplift of the failing core cylinder, (3) drainage of local pore pressures (i.e., the test can no longer be considered to be undrained), and (4) stick-slip behavior. Also, silts and sands provide increased friction effects. In light of these problems, and because of the expected disturbance during drilling, the shear vane test cannot be considered an accurate measure of the true shear strength of the sediment. In a laboratory situation, only properly controlled triaxial or simple shear tests can be used to provide in-situ strength adequately. The shear vane test, however, does provide an estimate of strength and a means for comparing downcore with between-hole parameters.

Compressional Wave Velocity

In addition to the continuous measurements made by the PWL/MST, discrete compressional-wave (P-wave) velocity measurements were obtained using one of two different systems during Leg 145, depending on the degree of lithification of the sediment. P-wave velocities were measured in unconsolidated sediment using a digital sound velocimeter (DSV; Mayer et al., 1988). The system used during Leg 145 was provided by the Department de Géologie Dynamique, Université de Paris VI and funded by CNRS, France. Velocity calculation is based on the accurate measurement of the time of flight of an impulsive acoustic signal traveling between a pair of piezoelectric transducers inserted in the split sediment cores. The signal used was a 2-μs square wave; the transducers had resonances at about 250 and 750 kHz. A dedicated microcomputer controlled all functions of the velocimeter. The transmitted and received signals were digitized by a Nicolet 320 digital oscilloscope and transferred to the microcomputer for processing. The DSV software selected the first arrival and calculated sediment velocity; the full waveform was stored for later calculation of attenuation.

Two transducers, separated by approximately 7 cm, were used to measure the vertical (along the core axis) P-wave velocity. The transducers were firmly fixed at one end on a steel plate so their separation did not change during velocity determinations. An external digital thermometer was used to monitor the ambient temperature during measurements.

Periodically, the separation was evaluated precisely by running a calibration procedure in distilled water. A value for the sound velocity in distilled water was determined (based on standard equations) for the measured temperature, with the computer calculating the transducer separation using the signal traveltime. At each sampling interval (usually two per section), the transducers were carefully inserted into the split section, and velocity then measured.

The Hamilton Frame velocimeter was used to measure compressional-wave velocities at 500 kHz in discrete indurated sediment samples, and basement rocks. Samples were cut carefully using a double-bladed diamond saw. Sample thickness was measured directly from the velocimeter-frame lead screw. Zero traveltimes for the velocity transducers were estimated by linear regression of traveltime vs. distance for a series of aluminum and lucite standards. Filtered seawater was used to improve the acoustic contact between the sample and the transducers. The DSV oscilloscope and processing software were used to digitize waveforms, to calculate velocities, and to store the waveforms for later attenuation calculations.

Index Properties

Index properties (wet-bulk density, grain density, water content, porosity, and dry-bulk density) were calculated from measurements of wet and dry weights and dry volume. Samples of approximately 10 cm^3 were taken for determining of index properties. Soft sediment samples were placed in pre-calibrated aluminum containers prior to measuring weight and volume. Index properties measurements for lithified sediment and basement rock samples were measured in crushed portions of the sample cubes cut for determining velocity.

Sample weights were determined aboard the ship to a precision of ±0.01 g using a Scientech/Cahn electronic balance. Volumes were determined using a Quantachrome penta-pycnometer, a helium-displacement pycnometer. The Quantachrome pycnometer measures volumes to an approximate precision of 10^{-4} cm^3.

Frequent decreases in air pressure in the laboratory stack from opening the outside doors were observed to affect the performance of the pycnometer. Another problem that arose with the consistency of measurements was the result of slightly different pressures measured during different calibration runs. The variability associated with decrease in pressure was minimized by repeating the measurements until two volumes for the same cell agreed to within 0.05 cm^3. To correct for the differences associated with changes in calibration pressure, a standard was included in every other pycnometer run. The standard was rotated through each of the cells so that changes in the cells could be monitored. The sample volumes were then corrected for deviations from the known standard volume.

Based upon data from previous ODP legs, the dry volumes measured by the pycnometer were determined to be more accurate than the wet volumes, owing to the presence of volatiles in the wet samples that result in erroneous pressure readings. Therefore, only dry samples were run through the pycnometer during Leg 145. Dry weight and volume measurements were obtained after the samples were oven-dried at 110°C for 24 hr and allowed to cool in a desiccator. A salt correction assuming 35 ppt interstitial fluid salinity was applied to density and porosity computations, as described in Hamilton (1971).

Wet-bulk density was calculated from wet and dry weights and dry volumes. The wet volume, used to calculate bulk density, was calculated by adding the weight of the water lost through drying of the sample to that of the dry volume, using the following equation:

$$V_w = V_d + (W_w - W_d)/\rho_f \qquad (2)$$

where ρ_f is the density of evaporated water (assumed to equal 1.0); V_w is the calculated wet volume; W_w is the wet sample weight; W_d is the dry sediment weight, including the weight of the remaining salt; and V_d is the dry volume, including both the volume of the sediment or rock constituents and the volume of salt remaining in the sample after drying. Then, the wet bulk density is calculated in the normal manner, as follows:

$$\rho bw = W_w/V_w \qquad (3)$$

Porosity, water content (calculated as a percentage of dry weight), grain density, and dry-bulk density also were calculated using this calculated wet volume, according to the equations of Boyce (1976).

DOWNHOLE MEASUREMENTS

Introduction

Downhole logs can be used to characterize the geophysical, geochemical, and structural properties of a drilled sequence. Log measurements have several distinct advantages over core-based measurements: (1) they represent continuous, in-situ measurements of the formation, (2) they are multivariate and rapid to collect, and (3) they are unaffected by problems of incomplete and preferential core recovery that inhibit core-based studies.

After coring is completed, the hole is flushed of debris and a combination of sensors is lowered down the hole on a seven-conductor cable. Under rough sea conditions, a wireline heave motion compensator is employed to minimize the effect of ship's heave on the tool's position in the borehole. The sensors continuously monitor geophysical and geochemical property variations of the formation; these are recorded at depth increments of 15 cm using the Schlumberger cyber service unit (CSU) computer. The in-formation depth of investigation and vertical resolution are sensor-dependent, but are typically between 50 and 100 cm. Four different Schlumberger tool strings were used during Leg 145: (1) a seismic stratigraphic tool string, (2) a lithoporosity tool string, (3) the formation microscanner (FMS), and (4) the geochemical tool string. A schematic diagram of these four tool strings is shown in Figure 13. The first two tool strings frequently are combined to form the Quad combination tool string. The Lamont-Doherty temperature tool was attached to the base of each tool string to monitor borehole temperature variations.

Quad Combination Tool String

The Quad combination tool string employed during Leg 145 comprises four sensors: (1) the natural gamma-ray spectrometry tool (NGT), (2) the phasor dual-induction tool (DIT), (3) the long-spacing digital sonic tool (SDT), and (4) the high-temperature lithodensity tool (HLDT). The Quad combination tool string is designed to measure compressional-wave velocity; deep, intermediate, and shallow resistivities, and formation density in a single logging pass. Sonic velocity data are combined with density measurements to calculate an impedance log and to generate synthetic seismograms for the logged sequence. The NGT is run on all three tool strings to provide a common basis for log correlations.

The DIT provides three measurements of electrical resistivity, all having different radial depths of investigation. Two induction devices ("deep" and "medium" resistivities) send high-frequency alternating current through transmitter coils, creating a magnetic field that induces a secondary (Foucault) current in the formation. This ground-loop current produces a new inductive signal, proportional to the conductivity of the formation. This inductive signal is recorded by a series of receiving coils and is then converted to resistivity values. A third device, the spherically focused resistivity tool (SFL), measures the current necessary to maintain a constant voltage potential across a fixed interval. Vertical resolution is 2 and 1.5 m for the deep and medium inductions and 0.75 m for the SFL. These data are corrected for irregularities in borehole diameter.

Resistivity varies as a function of the inverse square root of porosity (Archie, 1942). Fluid salinity, clay content, hydrocarbon content, and temperature also are important factors influencing electrical resistivity. Other factors that may affect the measured resistivity are the concentration of hydrous and metallic minerals, formation porosity, and the geometry of the pore space.

The SDT records the time required for sound to travel along the borehole wall from one of two acoustic transmitters to two receivers over source-receiver distances of 8, 10, and 12 ft (2.4, 3.0, and 3.6 m). First arrivals for the individual source-receiver paths are used to calculate sonic velocities; four velocity values are measured at each depth, along four possible paths. Only compressional-wave velocities are determined on board the ship, but the complete sonic waveforms are recorded for post-cruise processing to determine shear wave and Stoneley wave velocities. The vertical resolution of the tool is approximately 2 ft (0.61 m). Logs can be corrected for cycle skipping (where the receiver misses the first arrival and responds to that of the second signal) using four-fold measurement redundancy. Compressional-wave velocity is controlled primarily by density and lithification; decreases in density and increases in consolidation and lithification typically result in velocity increases with depth in a sedimentary deposit.

The HLDT uses a ^{137}Ce source of 0.66 MeV gamma rays for measuring formation bulk density. This source is mounted in the tool body, and an eccentralizing arm presses it and a pair of detectors against the borehole wall. Determination of density is based on Compton scattering of gamma rays within the formation, which is a function of electron density. The electron density is converted to bulk density by assuming that most rock-forming elements have atomic weights that are twice their atomic numbers. In addition, the HLDT records a photoelectric effect index. Photoelectric absorption occurs in the energy window below 150 MeV and is principally dependent upon the energy of the incident gamma rays and the atomic cross section. This measurement is independent of porosity and therefore can be used as a matrix lithology indicator. Measurements of density and photoelectric effect require good contact between the sensor and borehole wall; the tool measures the "standoff," and can be corrected for excessive borehole roughness. The intrinsic vertical resolution of the tool is approximately 0.4 m.

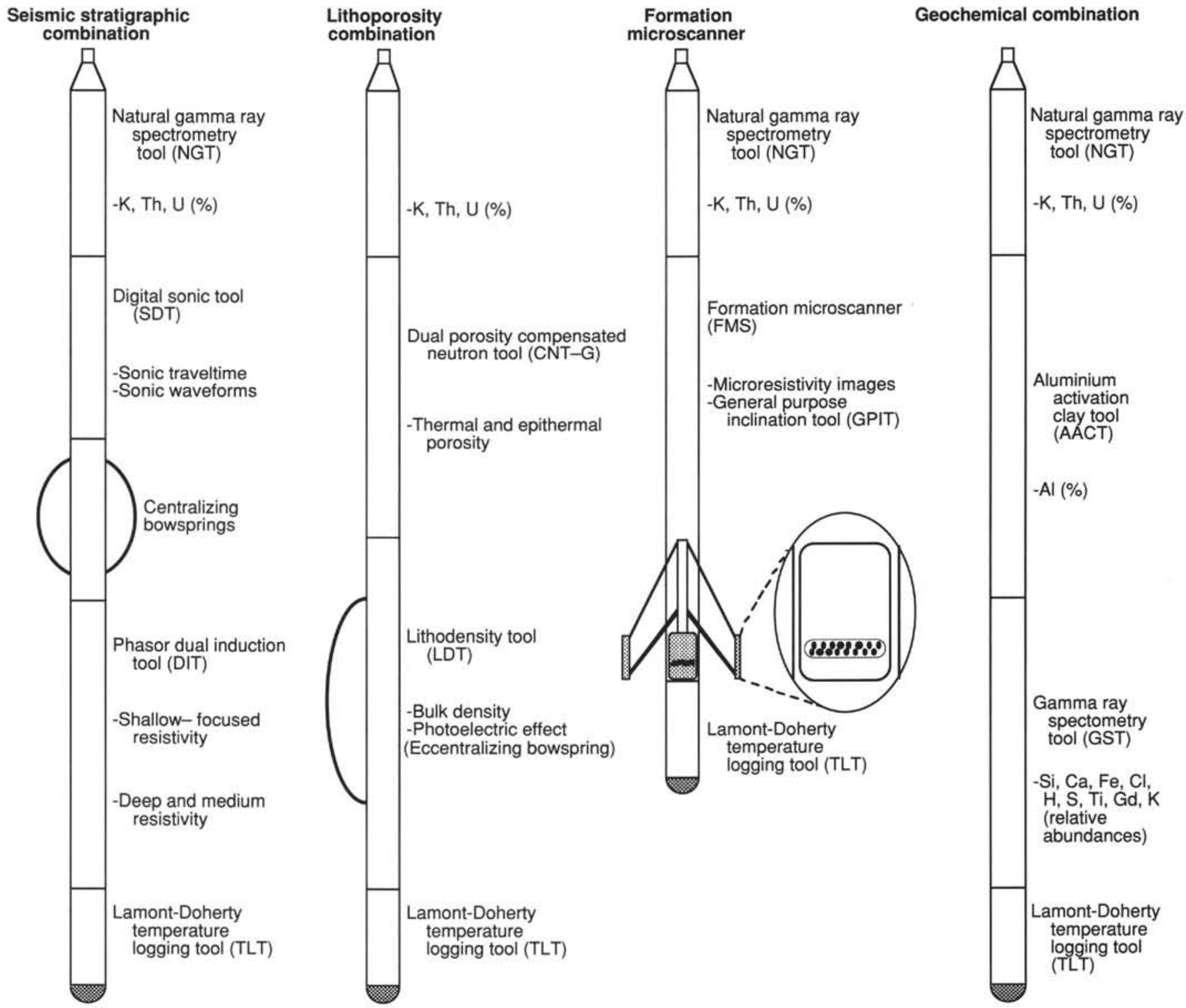

Figure 13. Schematic diagrams of Schlumberger logging tool strings used during Leg 145. Tool strings are not drawn to relative scale.

Geochemical Tool String

The geochemical tool string used during Leg 145 included an NGT, a gamma-ray spectrometry tool (GST), and an aluminum activation clay tool (AACT) (Hertzog et al., 1989). Relative concentrations of Si, Ca, Fe, S, H, and Cl and wet weight percentages of K, U, Th, and Al were determined on board the ship. Extensive additional shore-based processing was required to obtain dry weight percentages of the above elements, at which stage Gd and Ti abundances are also determined.

The NGT measures the natural radioactivity of the formation (Lock and Hoyer, 1971). Most natural gamma rays are emitted by ^{40}K and by U and Th isotopes and their daughter products. Near-field (i.e., near the borehole wall) natural gamma-ray emissions of the formation are measured by a NaI scintillation detector mounted inside the sonde. The energy spectrum measured by the detector is divided into five discrete energy windows. At each 15-cm sample interval, the total counts recorded in each window are processed to give elemental abundances of K, U, and Th. The in-formation depth of investigation is about 0.15 m. The NGT is positioned at the top of the tool string, and measures the natural radioactivity before the formation is irradiated by the sources in the tools below.

K, U, and Th are generally most abundant in clay minerals; thus, the gamma-ray log is commonly used as an estimate of the clay content of the formation. Silicic volcaniclastic material and K-feldspar-rich rocks also can have high concentrations of these three elements; thus, interpretations must be tied to the core lithology. At some sites, the U log closely follows variations in organic carbon content.

The AACT forms the second part of the geochemical tool string, and measures the concentration of Al in the formation by delayed neutron activation (Scott and Smith, 1973). When the natural isotope ^{27}Al absorbs a thermal neutron derived from the 2.5 MeV ^{252}Cf source of the AACT, it forms an unstable ^{28}Al atom having a half-life of about 2 min. When the unstable nucleus decays (to ^{28}Si), a gamma ray having a characteristic energy (1779 KeV) is emitted and subsequently detected by the AACT. Because the AACT simultaneously counts the natural gamma radiation of the formation, the net Al spectrum is determined by subtracting the count rates from the NGT, which is positioned above the AACT in the tool string.

The GST consists of a pulsed 14 MeV neutron generator and a NaI scintillation detector. Incident neutrons lose energy through inelastic scattering interactions and, on reaching thermal energy levels, are captured by elemental nuclei. Characteristic gamma rays are emitted upon neutron capture; these gamma rays and their relative energy levels are recorded by the tool. The 256-channel energy spectrum is deconvolved to determine relative abundances of Ca, Si, Fe, Cl, H, and S on board the ship. The post-cruise processing of the GST data provides the additional elemental yields of Gd and Ti. The above yields (except for Cl and H) are then combined with elements determined from the NGT and AACT to derive the dry weight percentages of the elements Si, Ca, Fe, S, Ti, K, and Al, in addition to Gd, Th, and U (in ppm). An estimate of (Mg + Na) can be made by using the photoelectric factor from the HLDT.

Formation Microscanner

The formation microscanner (FMS) produces high-resolution images of the microresistivity character of the borehole wall that can be used for detailed sedimentological and/or structural interpretations (Ekstrom et al., 1986). The FMS tool comprises 16 electrode "buttons" on four orthogonal pads that are pressed against the borehole wall. The electrodes are spaced approximately 2.5 mm apart and are arranged in two diagonally offset rows of eight electrodes each. Processing corrects the offset rows to one level, doubling the horizontal resolution to approximately 1.25 mm. The FMS tool string contains a general purpose inclinometry tool (GPIT) that orients the resistivity measurements through the combinated use of an accelerometer and magnetometer data. This tool string includes an NGT to permit correlation to other tool strings. The raw data are processed at sea to transform individual microresistivity traces into complete, oriented images. Complete color images can be made available to shipboard scientists within 2 to 3 days after logging.

Applications of the FMS logs include detailed correlation of coring and logging depths; orientation of cores; mapping of fractures, faults, foliations, and other formation structures; as well as determination of strikes and dips of bedding planes. In addition, the FMS can be used to estimate and stress in the borehole with precise measurements of borehole diameter in two orthogonal directions. In an isotropic, linearly elastic rock subjected to an anisotropic stress field, breakouts form along the borehole wall as a result of compressive stress that exceeds the strength of the rock. Under these conditions, the breakout orientation develops in the direction of the least principal horizontal stress. Stress orientations deduced from breakouts have been demonstrated to be consistent with other independent stress indicators (Bell and Gough, 1979; Zoback et al., 1988).

The Barnes/Uyeda and Lamont Temperature Tools

The Barnes/Uyeda water sampler and temperature probe (WSTP) allows for temperatures to be measured and pore waters to be sampled in shallow unconsolidated or semiconsolidated sediments. This probe is mounted on the end of the APC-coring device, lowered on the sand line, and latched onto the drilling shoe; it is then pressed ~1 m into the undisturbed sediments directly below the drill bit. The probe is left in position for 15 to 20 min to allow for equilibration and then is retrieved. The temperature data are recorded internally. Although the water sampler portion of the tool was not used during Leg 145, temperature measurements were used to determine the vertical temperature gradients in the sediments, and together with measurements of thermal conductivity were used to determine heat flow.

The Lamont temperature logging tool (TLT) is a self-contained tool that can be attached to the base of any of the sensor combinations. Data from two thermistors and a pressure transducer are collected every 0.5 s and are internally recorded. Once the in-situ measurement is completed, the data are transferred to a shipboard computer for analysis. The fast-response thermistor, though less accurate, is able to detect small, abrupt increases in temperature caused by fluid flow from the formation. The slow-response thermistor is more accurate and can be used to estimate the temperature gradient. Data are recorded as a function of time, with conversion to depth based on the pressure transducer. Unlike the Barnes/Uyeda probe, the TLT measures borehole water temperature; rather than formation temperature, so one commonly observes a gradual warming of the TLT temperatures as logging proceeds. Hence, the most reliable TLT temperatures are those taken from the last logging run, and even these should be considered minimum estimates.

Magnetic Remanence and Susceptibility Logging Tools

In a borehole, rocks are still close to their natural equilibrium state, so few secondary remagnetizations (such as weathering) are expected. High-sensitivity total magnetic field and susceptibility logging tools were deployed during Leg 145 to test the effectiveness of these tools for resolving borehole magnetic polarity transitions and susceptibility variations. These tools were developed jointly by the oil industry (TOTAL) and French government research institutions (CEA-LETI and CNRS-ENS). The tools were constructed by CEA-LETI, a branch of the French Atomic Energy Commission, which also developed the technical solutions (Pocachard et al., 1991).

The magnetometer measures the total induction, $B = \mu_0(H + [J_i + J_r])$ (SI units), which is commonly and incorrectly referred to as "Earth's magnetic field." B (Earth's total induction) is expressed in nannoteslas (nT) and is the induction that results either from a magnetic field, H (Earth's field, in that case) and/or from an induced magnetization, J_i, or remanent magnetization, J_r, both expressed in amperes per meter (A/m), with μ_0 being the permeability of a vacuum.

Magnetic induction B in a borehole depends on location p and time t, with (Pozzi et al., 1988):

$$B(p,t) = B_r(p) + B_a(p) + B_f(p) + B_t(p,t). \quad (5)$$

$B_r(p)$ is the regular inner field, whereas $B_a(p)$ is the anomaly field related to large-scale heterogeneities in susceptibility or in magnetic remanence. In the absence of such heterogeneities in the vicinity of the borehole, the spatial variation of both B_r and B_f with depth is linear. $B_r(z)$ can be sufficiently estimated by assuming that the main regular field is dipolar. In such an approximation, one can express this at sea level as,

$$Br_0 = M\mu_0 (3 \cos^2 \theta + 1)^{1/2}/4 \pi R^3 \quad (6)$$

with M = the moment of the equivalent dipole; θ = co-latitude, and R = Earth's radius. Accordingly, the magnetic gradient with depth will be equal to $-3\, Br_0/R$ (about 22 nT/km), with Br_0 increasing with depth. $B_f(p)$ is the induction from the magnetization (induced and remanent) of the sediments around the borehole and can easily be separated from $B_r(p)$ and $B_a(p)$. $B_t(p,t)$ is time dependent and represents the induction caused by transient variations of Earth's magnetic field. The time-dependent component can be reduced using a radiolinked reference, or it can be estimated by repeat sections. To obtain direct magnetostratigraphy from $B_f(p)$ the susceptibility and total field measurements are combined to discriminate induced from remanent magnetizations. Specifications of the probes (such as impulse response, calibration ratio, and geomagnetic location of the hole) are used to calculate the susceptibility effect on the scalar total field magnetometer. The result of these calculations is the scalar remanent magnetization.

The nuclear resonance magnetometer tool (NRMT) can be used in borehole temperatures up to 125°C; however, the probe used for Leg 145 is more precise and has a maximum operating temperature of 65°C. Average precision of this tool is 0.5 nT, based on repeat sections. In the absence of a radiolinked reference, a whole repeat section is needed to estimate the different components of the Earth's induction.

The susceptibility magnetic tool (SMT) employs a classic measurement principle that detects the mutual induction signal between two coils (0.8 m apart) caused by the surrounding borehole lithology. The excitation frequency is about 200 Hz. Measurement precision between repeated sections is generally better than 3 ppm (3×10^{-6} SI). A repeat section is necessary to remove thermal drift effects from the measurements. Both tools are housed by nonmagnetic materials; tools are logged at 550 m/hr, and the data are recorded every 5 cm. Time constraints did not allow us to use this speed for the susceptibility tool. Thus, only partial repeat sections have been recorded at the highest 1100 m/hr speed. These tools have already been run in numerous holes, including those drilled during Leg 134 Site 833. The magnetostratigraphic interpretation of the recorded logs usually gives good results when compared to those obtained using plugs taken from cores recovered in the same hole (Pozzi et al., in press), and correlations among oil wells up to 80 km apart in the Paris Basin have been possible.

REFERENCES*

Akiba, F., 1985. Middle Miocene to Quaternary diatom biostratigraphy in the Nankai Trough and Japan Trench, and modified lower Miocene through Quaternary diatom zones for the middle- to high-latitudes of the North Pacific. *In* Kagami, H., Karig, D.E., Coulbourn, W.T., et al., *Init. Repts. DSDP,* 87:393–481.

Archie, G.E., 1942. The electrical resistivity log as an aid in determining some reservoir characteristics. *J. Pet. Tech.,* 5:1–8.

Backman, J., 1896. Late Paleocene to middle Eocen calcareous nannofossil biostratigraphy from the Shatsky Rise, Walvis Ridge and Italy. *Palaeogeogr., Palaeoclimatol., Palaeoecol.,* 57:43–59.

Backman, J., and Shackleton, N.J., 1983. Quantitative biochronology of Pliocene and early Pleistocene calcareous nannofossils from the Atlantic, Indian, and Pacific oceans. *Micropaleont.,* 8:141–170.

Backman, J., and Pestiaux, P., 1986. Pliocene discoaster abundance variations, Deep Sea Drilling Project Site 606: biochronology and paleoenvironmental implications. *In* Ruddiman, W.F., Kidd, R.B., Thomas, E., et al., *Init. Repts. DSDP,* 94 (Pt. 2): Washington (U.S. Govt. Printing Office), 903–910.

Backman, J., Schneider, D.A., Rio, D.m, and Okada, H., 1990. Neogene low-latitude magnetostratigraphy from Site 710 and revised age estimates of Miocene nannofossil events. *In* Backman, J., Duncan, R.A., et al., *Proc. ODP, Sci. Results,* 115: College Station, TX (Ocean Drilling Program), 271–276.

Baldauf, J.G., and Barron, J.A., 1991. Diatom biostratigraphy: Kerguelen Plateau and Prydz Bar regions of the Southern Ocean. *In* Barron, J.A., Larsen, B., et al., *Proc. ODP, Sci. Results,* 119: College Station, TX (Ocean Drilling Program), 547–598.

Barron, J.A., 1980. Lower Miocene to Quaternary diatom biostratigraphy of Leg 57, off Northeastern Japan, Deep Sea Drilling Project. *In* von Huene, R., Nasu, N., et al., *Init. Repts. DSDP,* 56, 57 (Pt. 2): Washington (U.S. Govt. Printing Office), 641–685.

————, 1992. Neogene diatom datum levels in the equatorial and North Pacific. *In* Ishizaki, K., and Saito, T. (Eds.), *The Centenary of Japanese Micropaleontology*: Tokyo (Tokyo Univ. Press), 413–425.

Bell, J.S., and Gough, D.I., 1979. Northeast-southwest compressive stress in Alberta: evidence from oil wells. *Earth Planet. Sci. Lett.,* 45:475–482.

Berggren, W.A., Kent, D.V., and Flynn, J.J., 1985. Jurassic to Paleogene: Part 2. Paleogene geochronology and chronostratigraphy. *In* Snelling, N.J. (Ed.), *The Chronology of the Geological Record.* Geol. Soc. London Mem., 10:141–195.

Berggren, W.A., Kent, D.V., and Van Couvering, J.A., 1985. The Neogene: Part 2. Neogene geochronology and chronostratigraphy. *In* Snelling, N.J. (Ed.), *The Chronology of the Geological Record.* Geol. Soc. London Mem., 10:211–260.

Blow, W.H., 1969. Late middle Eocene to Recent planktonic foraminiferal biostratigraphy. *Proc. 1st Int. Conf. Planktonic Microfossils* (Geneva 1967), 1:199–422.

Bodén, P., in press. Taxonomy and stratigraphic occurrence of *Thalassiosir tetraoestruppi* sp. nov. and related species in upper Miocene and lower Pliocene sediments from the Norwegian Sea, North Atlantic and Northwest Pacific. *Terra Nova.*

Bougault, H., Cambon, P., and Toulhoat, H., 1977. X-ray spectrometric analysis of trace elements in rocks: correction for instrumental interferences. *X-Ray Spectrom.,* 6:66–72.

Boyce, R.E., 1976. Definitions and laboratory techniques of compressional sound velocity parameters and wet-water content, wet-bulk density, and porosity parameters by gravimetric and gamma ray attenuation techniques. *In* Schlanger, S.O., Jackson, E.D., et al., *Init. Repts. DSDP,* 33: Washington (U.S. Govt. Printing Office), 931–958.

————, 1977. Deep Sea Drilling Project procedures for shear strength measurement of clayey sediment using modified Wykeham Farrance laboratory vane apparatus. *In* Barker, P., Dalziel, I.W.D., et al., *Init. Repts. DSDP,* 36: Washington (U.S. Govt. Printing Office), 1059–1068.

Brindley, G.W., and Brown, G. (Eds.), 1980. *Crystal Structures of Clay Minerals and Their X-ray Identification.* Mineral. Soc. Monogr., 5.

Cande, S.C., and Kent, D.V., 1992. A new geomagnetic polarity timescale for the Late Cretaceous and Cenozoic. *J. Geophys. Res.,* 97:13917–13951.

Ekstrom, M.P., Dahan, C.A., Chen, M.-Y., Lloyd, P.M., and Rossi, D.J., 1986. Formation imaging with microelectrical scanning arrays. *Trans. SPWLA 27th Ann. Logging Symp.,* Pap. BB.

Emeis, K.-C., and Kvenvolden, K.A., 1986. Shipboard organic geochemistry on *JOIDES Resolution. ODP Tech. Note,* 7.

Fisher, R.V., and Schmincke, H.-U., 1984. *Pyroclastic Rocks:* New York (Springer-Verlag).

Foreman, H.P., 1975. Radiolaria from the North Pacific, Deep Sea Drilling Project, Leg 32. *In* Larson, R.L., Moberly, R., et al., *Init. Repts. DSDP,* 32: Washington (U.S. Govt. Printing Office), 579–676.

Fornaciari, E., Raffi, I., Rio, D., Backman, J., and Olafsson, G., 1990. Quantitative distribution patterns of Oligocene and Miocene calcareous nannofossils from the Western Equatorial Indian Ocean. *In* Duncan, R.A., Backman, J., Peterson, L.C., et al., *Proc. ODP, Sci. Results,* 115: College Station, TX (Ocean Drilling Program), 237–254.

Gersone, R., and Burckle, L.H., 1990. Neogene diatom biostratigraphy of ODP Leg 113, Weddell Sea (Antarctic Ocean). *In* Barker, P.F., Kennett, J.P., et al., *Proc. ODP, Sci. Results,* 113: College Station, TX (Ocean Drilling Program), 761–789.

Gieskes, J.M., Gamo, T., and Brumsack, H.J., 1991. Chemical methods for interstitial water analysis aboard *JOIDES Resolution. ODP Tech. Note,* 15.

Hamilton, E.L., 1971. Prediction of in-situ acoustic and elastic properties of marine sediments. Geophysics, 36:266–284.

Harwood, D.M., and Maruyama, R., 1992. Middle Eocene to Pleistocene diatom biostratigraphy of Southern Ocean sediments from the Kerguelen Plateau, Leg 120. *In* Wise, S.W., Jr., Schlich, R., et al., *Proc. ODP, Sci. Results,* 120: College Station, TX (Ocean Drilling Program), 683–733.

Hay, W.W., 1970. Calcareous nannofossils from cores recovered on DSDP Leg 4. *In* Bader, R.G., Gerard, R.D., et al., *Init. Repts. DSDP,* 4: Washington (U.S. Govt. Printing Office), 455–501.

Hays, J.D., 1970. Stratigraphy and evolutionary trends of Radiolaria in North Pacific deep sea sediments. *In* Hays, J.D. (Ed.), *Geological Investigations of the North Pacific.* Mem.—Geol. Soc. Am., 126:185–218.

Hays, J.D., and Shackleton, N.J., 1976. Globally synchronous extinction of the radiolarian *Stylatractus universus. Geology,* 4:649–652.

Hertzog, R., Colson, L., Seeman, B., O'Brien, M., Scott, H., McKeon, D., Wraight, J., Grau, J., Ellis, D., Schweitzer, J., and Herron, M., 1989. Geochemical logging with spectrometry tools. *SPE Form. Eval.,* 4:153–162.

Johnson, D.A., and Nigrini, C.A., 1985. Synchronous and time-transgressive Neogene radiolarian datum levels in the equatorial Indian and Pacific oceans. *Mar. Micropaleontol.,* 9:489–523.

Johnson, D.A., Schneider, D.A., Nigrini, C.A., Caulet, J.P., and Kent, D.V., 1989. Pliocene-Pleistocene radiolarian events and magnetostratigraphic calibrations for the tropical Indian Ocean. *Mar. Micropaleontol.,* 14:33–66.

Kennett, J.P., and Srinivasan, M.S., 1983. *Neogene Planktonic Foraminifera*: New York (Hutchison-Ross).

Kent, D.V., and Gradstein, F.M., 1985. A Cretaceous and Jurassic geochronology. *Geol. Soc. Am. Bull.,* 96:1419–1427.

Koizumi, I., 1992. Diatom biostratigraphy of the Japan Sea: Leg 127. *In* Pisciotto, K.A., Ingle, J.C., Jr., von Breymann, M.T., Barron, J., et al., *Proc. ODP, Sci. Results,* 127/128 (Pt. 1): College Station, TX (Ocean Drilling Program), 249–289.

Koizumi, I., and Tanimura, Y., 1985. Neogene diatom biostratigraphy of the middle latitude western North Pacific, Deep Sea Drilling Project Leg 86. *In* Heath, G.R., Burckle, L.H., et al., *Init. Repts. DSDP,* 86: Washington (U.S. Govt. Printing Office), 269–300.

* Abbreviations for names of organizations and publication titles in ODP reference lists follow the style given in *Chemical Abstracts Service Source Index* (published by American Chemical Society).

Kvenvolden, K.A., and McDonald, T.J., 1986. Organic geochemistry on the *JOIDES Resolution*—an assay. *ODP Tech. Note,* 6.

Lock, G.A., and Hoyer, W.A., 1971. Natural gamma-ray spectral logging. *Log Analyst,* 12:3–9.

Manheim, F.T., and Sayles, F.L., 1974. Composition and origin of interstitial waters of marine sediments based on deep sea drill cores. *In* Goldberg, E.D. (Ed.), *The Sea* (Vol. 5): New York (Wiley Interscience), 527–568.

Martini, E., 1971. Standard Tertiary and Quaternary calcareous nannoplankton zonation. *In* Farinacci, A. (Ed.), *Proc. 2nd Int. Conf. Planktonic Microfossils Roma:* Rome (Ed. Tecnosci.), 2:739–785.

Mayer, L.A., Courtney, R.C., and Moran, K., 1987. Ultrasonic measurements of marine sediment properties. *Proc. Oceanogr.,* 87:139.

Mazzullo, J.M., Meyer, A., and Kidd, R., 1987. New sediment classification scheme for the Ocean Drilling Program. *In* Mazzullo, J., and Graham, A.G. (Eds.), *Handbook for Shipboard Sedimentologists.* ODP Tech. Note, 8:45–67.

Morley, J.J., 1985. Radiolarians from the Northwest Pacific, Deep Sea Drilling Project Leg 86. *In* Heath, G.R., Burckle, L.H., et al., *Init. Repts.* DSDP, 86: Washington (U. S. Govt. Printing Office), 399–422.

Morley, J.J., Hays, J.D., and Robertson, J.H., 1982. Stratigraphic framework for the late Pleistocene in the northwestern Pacific Ocean. *Deep-Sea Res.,* 19:1485–1499.

Nigrini, C.A., 1985. Radiolarian biostratigraphy in the central equatorial Pacific, Deep Sea Drilling Project Leg 85. *In* Mayer, L., Theyer, F., Thomas, E., et al., *Init. Repts. DSDP,* 85: Washington (U.S. Govt. Printing Office), 511–551.

Olafsson, G., 1991. Quantitative calcareous nannofossil biostratigraphy and biochronology of early through late Miocene sediments from DSDP Hole 608. *Meddel. Stockholms Univers. Insti. Geol. Geochem., Nr. 285, Pap. 4.*

Pocachard, J., Thomas, T., Barthès, V., Pagès, G., 1991. High resolution logging tool for borehole measurements of magnetization. *IUGG, XX Assembly,* Vienna.

Pozzi, J.-P., Barthes V., Thibal J., Pocachard J., Lim, M., and Pages, G., in press. Downhole magnetostratigraphy in sediments: comparison with the paleomagnetism of a core. *J. Geophys. Res.*

Pozzi, J.-P., Martin, J.P., Pocachard, J., Feinberg, H., and Galdeano, A., 1988. In situ magnetostratigraphy: interpretation of magnetic logging in sediments. *Earth Planet. Sci. Lett.,* 88:357–373.

Ratcliffe, E.H., 1960. The thermal conductivities of ocean sediments. *J. Geophys. Res.,* 65:1535–1541.

Reynolds, R.A., 1980. Radiolarians from the western North Pacific, Leg 57, Deep Sea Drilling Project. *In* Shipboard Scientific Party, *Init. Repts. DSDP,* 56, 57 (Pt. 2): Washington (U.S. Govt. Printing Office), 735–770.

Riedel, W.R., and Sanfilippo, A., 1970. Radiolaria, Leg 4, Deep Sea Drilling Project. *In* Bader, R.G., Gerard, R.D., et al., *Init. Repts. DSDP,* 4: Washington (U.S. Govt. Printing Office), 503–575.

————, 1971. Cenozoic radiolaria from the western tropical Pacific, Leg 7. *In* Winterer, E.L., Riedel, W.R., et al., *Init. Repts. DSDP,* 7 (Pt. 2): Washington (U.S. Govt. Printing Office), 1529–1672.

————, 1978. Stratigraphy and evolution of tropical Cenozoic radiolarians. *Micropaleontology,* 24:61–96.

Rio, D., Backman, J., and Raffi, I., in press. *Calcareous Nannofossil Biochronology and the Pliocene/Pleistocene Boundary:* Cambridge (Cambridge Univ. Press).

Rio, D., Raffi, I., and Villa, J., 1990. Pliocene-Pleistocene calcareous nannofossil distribution patterns in the western Mediterranean. *In* Kastens, K.A., Mascle, J., et al., *Proc. ODP, Sci. Results,* 107: College Station, TX (Ocean Drilling Program), 513–533.

Rio, D., Fornaciari, E., and Raffi, I., 1990. Late Oligocene through early Pleistocene calcareous nannofossils from western Equatorial Indian Ocean (Leg 115). *In* Duncan, R.A., Backman, J., Peterson, L.C., et al., *Proc. ODP, Sci. Results,* 115: College Station, TX (Ocean Drilling Program), 175–235.

Sakai, T., 1980. Radiolarians from sites 434,435, and 436, Northwest Pacific Leg 56, Deep Sea Drilling Project. *In* von Huene, R., Nasu, N., et al., *Init. Repts. DSDP,* 56, 57 (Pt. 2): Washington (U.S. Govt. Printing Office), 695–733.

Sanfilippo, A., Westberg-Smith, M.J., and Riedel, W.R., 1985. Cenozoic radiolaria. *In* Bolli, H.M., Saunders, J.B., and Perch-Nielsen, K. (Eds.), *Plankton Stratigraphy:* Cambridge (Cambridge Univ. Press), 631–712.

Scott, H.D., and Smith, M.P., 1973. The aluminum activation log. *Log Analyst,* 14:3–12.

Shepard, F., 1954. Nomenclature based on sand-silt-clay ratios. *J. Sediment. Petrol.,* 24:151–158.

Shipboard Scientific Party, 1988. Explanatory notes: Leg 112. *In* Suess, E., von Huene, R., et al., *Proc. ODP, Init. Repts.,* 112: College Station, TX (Ocean Drilling Program), 25–44.

————, 1990. Explanatory notes. *In* Rangin, C., Silver, E.A., von Breymann, M.T., et al., *Proc. ODP, Init. Repts.,* 124: College Station, TX (Ocean Drilling Program), 7–33.

Shipboard Scientific Party, 1992. Explanatory notes. *In* Mayer, L., Pisias, N., Janecek, T., et al., *Proc. ODP, Init. Repts.,* 138: College Station, TX (Ocean Drilling Program), 13–41.

Sissingh, W., 1977. Biostratigraphy of Cretaceous calcareous nannoplankton. *Geol. Mijnbouw,* 56:37–65.

Spencer-Cervato, C., Lazarus, D.B., Beckman, J.-P., Perch-Nielsen, K., and Bolli, M., in press. New calibration of Neogene radiolatian events in the North Pacific. *Mar. Micropaleontol.,*

Thierstein, H.R., 1976. Mesozoic calcareous nannoplankton biostratigraphy of marine sediments. *Mar. Micropaleontol.,* 1:325–362.

Thierstein, H.R., Geitzenauer, K.R., Molfino, B., and Shackleton, N.J., 1977. Global synchroneity of late Quaternary coccolith datum levels: validation by oxygen isotopes. *Geology,* 5:400–405.

Vacquier, V., 1985. The measurement of thermal conductivity of solids with a transient linear heat source on the plane surface of a poorly conducting body. *Earth Planet. Sci. Lett.,* 74:275–279.

van Morkhoven, F.P.C.M., Berggren, W.A., and Edwards, A.S., 1986. Cenozoic cosmopolitan deep-water benthic foraminifera. *Bull. Cent. Rech. Explor.-Prod. Elf-Aquitaine,* Mem. 11.

Von Herzen, R.P., and Maxwell, A.E., 1959. The measurement of thermal conductivity of deep-sea sediments by a needle-probe method. *J. Geophys. Res.,* 64:1557–1563.

Weaver, F.M., Casey, R.E., and Perezm, A.M., 1981. Stratigraphic and paleoceanographic significance of early Pliocene to middle Miocene radiolarian assemblages from northern to Baja California. *In* Garrison, R.E., and Douglas, R.G. (Eds.), *The Monterey Formation and Related Siliceous Rocks of California*: Los Angeles (Pac. Sect. Soc. Econ. Paleontol. Mineral.), Spec. Publ., 71–86.

Wentworth, C.K., 1922. A scale of grade and class terms of clastic sediments. *J. Geol.,* 30:377–392.

Zijderveld, J.D.A., Zachariasse, J.W., Verhallen, P.J.J.M., and Hilgen, F.J., 1986. The age of the Miocene-Pliocene boundary. *Newsl. Stratigr.,* 16:169–181.

Zoback, M.D., Zoback, M.L., Mount, V.S., Suppe, J., Eaton, J.P., Healy, J.H., Oppenheimer, D., Reasenberg, P., Jones, L., Raleigh, C.B., Wong, I.G., Scotti, O., and Wentworth, C., 1988. New evidence on the state of stress of the San Andreas Fault. *Science,* 238:1105–1111.

Ms 145IR-104